Technische Universität München

Fachgebiet Strömungsmechanik

Prof. Dr.-Ing. Rainer Friedrich

Three-dimensional PDF simulation of a piloted turbulent non-premixed jet flame

Michael Stöllinger

Diplomarbeit

30. April, 2005

Advisor:

Prof. Dr.-Ing Rainer Friedrich

Prof. Dr. rer. nat. Stefan Heinz

Abstract

Turbulent combustion is an important process in many technical applications, e.g. industrial gas furnaces used for heating water, production of steam and combustion in jet and diesel engines. To control the turbulent combustion, simulation tools with predictive power are required. The basic equations for turbulent combustion are well known, but their application to the complex flows appearing in most technical applications is not possible with the speed and storage capacity of present day computers. To simulate complex turbulent flows, averaged equations together with turbulence models for the unclosed terms are used. In turbulent reactive flows, the averaged equations can be applied only for simplified chemistry. To describe turbulent combustion accurately, the inclusion of realistic chemical kinetics requires a stochastic model that describes the statistics of the complex turbulence-chemistry interaction.

To apply a stochastic model successfully in a turbulent combustion simulation, three problems have to be solved. Although theoretically arbitrary complex reaction mechanisms could be applied, they are numerically intractable and an appropriate, simplified chemistry scheme has to be found. The second problem of stochastic modelling is that the molecular species mixing appears in unclosed form. Different models are available, but their performance depends on the particular flow and the most appropriate one has to be selected. The third problem is that the solution of the stochastic model is computationally expensive and to reduce the computational time the simulations in most published research on turbulent combustion to date are two-dimensional. Since most of the flows in technical combustion devices are three-dimensional, the performance of the stochastic model for three-dimensional flows is an open question of research.

In this work, the three problems have been addressed and applied to the Delft III flame. The Delft III flame is a piloted, non-premixed, turbulent jet flame. The turbulent flow field can be reasonably well simulated with prescribed accuracy. Therefore, the results of different mixing models and chemistry schemes can be studied. The pilot flames used to stabilize the flame introduce three-dimensional effects; the structure of this flame is very similar to that of flames used in industrial combustion devices. The simulations have been performed in three-dimensions using the commercial CFD-package FLUENT. Developing the three-dimensional PDF model

was a great challenge. The model can be used for further simulations with improved mixing models and different chemistry schemes.

Acknowledgements

This work was supported by a project of the German Research Foundation (DFG transfer project 42) and FLUENT INC.

I want to thank my advisors, Prof. Dr. Rainer Friedrich and Prof. Dr. Stefan Heinz for their great support.

I also want to thank Prof. Dr. Bart Merci from the Ghent University and Prof. Dr. Dirk Roekaerts from the University of Delft for their advise and many suggestions.

Contents

Chapter 1

Introduction

1.1 Turbulent combustion

The discovery of how to ignite and use fire was one of the most important steps in the development of mankind. Fire heats our houses, it cooks our food and it is one of the most important sources in the production of electric energy. The most characteristic property of combustion processes such as fire and flames is the presence of rapid, exothermic chemical reactions. The presence of high temperatures in typical combustion situations causes a fast conversion from reactants to products. In addition to these chemical reactions, physical effects such as mass and heat transfer play an important role, especially in gaseous turbulent combustion. In this case the large scale convection and molecular and turbulent diffusion influences the progress of the chemical reactions. In general, turbulent combustion is characterized by the complex interaction between turbulent flow field and chemical reaction. The turbulent flow field yields to fluctuations in thermochemical scalars like the temperature, species concentration or species production rates. These quantities in turn, act on the flow field by changing the density. Therefore, the difficult part in describing turbulent combustion is to find a theory for the interacting chemical and physical processes. The research in the field of turbulent combustion is driven by the need for predictive tools in the design process of new, improved combustion devices. Turbulent combustion is found in many applications such as large scale thermal and electric power generation, four stroke engines and aircraft gas turbines. Nowadays, improvement in these applications of turbulent combustion does not only mean an increase of efficiency but also reduction of problematic exhaust gases such as CO and NO_x. Detailed knowledge on the physical and chemical processes in turbulent combustion can help to reduce these pollutant emissions.

1.2 Objective and approach

The objective of this study is to find and apply appropriate models that improve the simulation of turbulent combustion with the commercial CFD-package FLUENT. Special emphasize was given to the chemistry model, the mixing model describing the molecular mixing of species and the inclusion of three-dimensional effects.

In turbulent combustion, effects controlled by chemical kinetics such as local flame extinction and re-ignition are important. To include realistic chemical kinetic effects, a stochastic description of the turbulence-chemistry interaction is used. The stochastic description is based on the probability density function (PDF) of the scalar variables such as species concentration and temperature. The PDF completely determines the combined statistics of these scalars, especially the mean values and variances. The PDF can be obtained by solving a transport equation. The chemical reaction source term, describing the species conversion due to reaction, appears in closed form in this transport equation. Theoretically, arbitrarily complex chemical reaction schemes could be used but they are numerically not tractable. The first challenge in modelling turbulent combustion is to find an appropriate reduced chemical mechanism for the combustion problem considered.

In the PDF transport equation, the term describing the mixing of species at the molecular level (micro-mixing) appears in unclosed form and has to be modelled. The micro-mixing is crucial in turbulent combustion, because chemical reactions take place at molecular scales, when the molecules hit each other with sufficient kinetic energy. Different models for the micro mixing exist, but their performance depends on the problem considered. For a particular combustion problem, the best performing micro mixing has to be found to obtain improved results.

Solving the stochastic model for turbulent combustion is complex and computationally expensive. The simulations in most published research to date are performed in two-dimensions to reduce the computational time. The performance of the used models such as the micro mixing model in three-dimensional simulations has to be shown in order to use these models with confidence in prognosis applications. Most of the flows in technical applications are three-dimensional, simulating them in two-dimensions always implies a simplification. Three-dimensional simulations would help to decide whether or not such a simplification is justified.

The turbulent combustion problem considered in this thesis is the so-called Delft

III flame. This flame can be seen as laboratory scale model of turbulent flames as they are used in industrial applications. The Delft III flame is a turbulent, non-premixed, piloted jet flame with strong turbulence-chemistry interaction. The main fuel is natural gas and the oxidizer is air. The pilot flames, used to stabilize the main flame, also introduce three-dimensional effects. This flame is especially useful for studying the results of different micro mixing and chemistry models because the underlying flow field can be reasonably well described with standard turbulence models. The better the underlying flow field can be described, the clearer are the effects of mixing and chemistry models visible. Another reason for simulating the Delft III flame is that a detailed experimental database for the velocity and scalar values exists for this flame.

The three-dimensional simulations of the Delft III flame are performed using the commercial CFD-package FLUENT. The PDF-method is used to describe the turbulence-chemistry interaction. A skeletal chemical mechanism including 23 species and 104 elemental reactions is used to describe the chemical kinetics. Different mixing models have been used in the simulations. The simulations can be seen as a basic numerical setup for the Delft III flame. The developed three-dimensional model can be used for further simulations using new or improved mixing models and different chemistry schemes.

1.3 Outline of this thesis

This thesis can be divided into three parts. The first part deals with the transport equations, the stochastic modelling approach and the numerical techniques used for the prediction of the turbulent flame. Chapter 2 presents the governing, deterministic equations describing turbulent reactive flows. In chapter 3, a statistical description of turbulent reactive flows,the so-called PDF transport equations are presented. The numerical solution technique for the PDF transport equation is also presented in chapter 3.

The second part gives an overview of the chemistry models and the configuration of the Delft III flame. Chapter 4 gives a brief introduction into the technique to obtain simplified chemical mechanism. In chapter 5, details on the Delft III flame are presented. A presentation of two-dimensional simulations and the encountered

difficulties in these simulations are also given in chapter 4.

In the third and last part of the thesis, the three-dimensional model of the Delft III flame is presented in chapter 6. The thesis closes with a presentation of the simulation results and a discussion of the conclusions of this study in chapter 7.

Chapter 2

Deterministic flow equations

The basic equations that describe turbulent reactive flow can be derived from conservation laws for mass, momentum, energy and chemical species. Using the assumption of a Newtonian fluid and the equation of state for an ideal gas, the resulting system of nonlinear partial differential equations completely determines the turbulent flow field. Due to the complexity of the nonlinear, coupled partial differential equation system, known analytical solutions are restricted to simple non-reacting, laminar flows. In order to obtain solutions for more complex, turbulent reacting flows, numerical solution techniques are needed.

In this chapter, the basic equations of the instantaneous variables for turbulent reactive flows are presented. From these equations, the averaged equations are derived. The $k-\epsilon$ model is presented to close the Reynolds stress tensor. The chapter closes with a discussion about the closure problems of the averaged reaction rate.

2.1 Conservation equations for the instantaneous flow variables

The evolution of a turbulent reactive flow in space and time is governed by the conservation equations for mass, momentum, energy and species. The form of these equations and the approach to obtain differential equations from the integral relations can be found in many standard texts, e.g. WARNATZ et al. (1996). Conservation of mass is expressed by the continuity equation:

$$\frac{\partial \rho}{\partial t} + \frac{\partial (\rho U_i)}{\partial x_i} = 0 \tag{2.1}$$

in which ρ is the mass density, U_i the velocity and x_i the Cartesian coordinate with $i = 1, 2, 3$. Einstein's summation convention over repeated indices is applied.

Conservation of momentum in the x_j-direction yields

$$\rho\frac{\partial U_j}{\partial t} + \rho U_i\frac{\partial U_j}{\partial x_i} = -\frac{\partial p}{\partial x_j} + \frac{\partial \tau_{ij}}{\partial x_i} + \rho g_j. \tag{2.2}$$

Here, τ_{ij} denotes the viscous stress tensor, p the pressure and g_i the gravitational acceleration. Together, equations (2.1) and (2.2) are called the Navier-Stokes equations for low-Mach-number flows. The conservation equation for energy formulated in terms of the specific enthalpy h, is

$$\rho\frac{\partial h}{\partial t} + \rho U_i\frac{\partial h}{\partial x_i} = -\frac{\partial J_i^h}{\partial x_i}. \tag{2.3}$$

J_i^h denotes the molecular enthalpy flux. Radiative heat transfer is assumed to be negligible in the flame studied in this thesis. The radiative source term has therefore been omitted. Furthermore, the low-Mach-number assumption implies that the effects of viscous dissipation and transient pressure are neglected in the energy equation.

The conservation equation for a chemical species α expressed in terms of its mass fraction Y_α reads

$$\rho\frac{\partial Y_\alpha}{\partial t} + \rho U_i\frac{\partial Y_\alpha}{\partial x_i} = -\frac{\partial J_i^\alpha}{\partial x_i} + \rho S_\alpha, \quad \alpha = 1, 2, 3, ...n_s. \tag{2.4}$$

Here, J_i^α is the molecular flux of species α and S_α is the source term giving the net production of species α due to chemical reaction. The total number of species involved is n_s.

In addition to the conservation equations (2.1)-(2.4), an expression for the viscous stress tensor and equations describing the thermodynamic state are needed. For a Newtonian fluid the viscous stress tensor contains only simple shear effects and can be written as:

$$\tau_{ij} = -\mu\left(\frac{\partial U_i}{\partial x_j} + \frac{\partial U_j}{\partial x_i}\right) + \frac{2}{3}\mu\frac{\partial U_k}{\partial x_k}\delta_{ij} \tag{2.5}$$

in which μ is the dynamic viscosity. Assuming that the mixtures under investigation can be considered as ideal gases, the hydrodynamic equation of state is the gas law for multi-component mixtures,

$$p = \rho R_0 T\sum_{\alpha=1}^{n_s}\frac{Y_\alpha}{W_\alpha} \tag{2.6}$$

where R_0 is the universal gas constant, T the temperature of the mixture and W_α the molar mass of species α. The caloric equation of state relates the specific enthalpy (enthalpy per unit mass) to the temperature and reads

$$h = \sum_{\alpha=1}^{n_s} Y_\alpha \int_0^T c_{p,\alpha}(\theta) d\theta \tag{2.7}$$

where $c_{p,\alpha}$ is the temperature-dependent specific heat of species α.

The energy equation (2.3) and the equation describing conservation of species 2.4 have the same structure, except for the source term that is absent in the energy equation. The equations can be combined by defining the composition vector ϕ_i as

$$\phi_\alpha = Y_\alpha, \quad \alpha = 1, ..., n_s \quad \phi_{n_c} = h \tag{2.8}$$

with $n_c = n_s + 1$. The conservation equation for the n_c scalars thus becomes

$$\rho \frac{\partial \phi_\alpha}{\partial t} + \rho U_i \frac{\partial \phi_\alpha}{\partial x_i} = -\frac{\partial J_i^\alpha}{\partial x_i} + \rho S_\alpha, \quad \alpha = 1, 2, ...n_c. \tag{2.9}$$

with $J_i^{n_c} = J_i^h$ and $S_{n_c} = 0$.

Together with appropriate constitutive relations for J_i^h, J_i^α, $c_{p,\alpha}$ and a specification of the chemical source term S_α, the set of equation (2.1)-(2.7) provides a complete deterministic description of turbulent reactive flows. Numerical simulations which solve these equations for all scales of a turbulent flow, are called direct numerical simulations (DNS). The smallest scales in a turbulent flow field are given by the scales at which viscous dissipation of energy takes place, the so-called Kolmogorov scale. To cover all the dynamics of the flow, the discretization in space and time must be accurate and must resolve these smallest scales. For a fully three-dimensional simulation this means that the required computer storage scales as $Re^{\frac{9}{4}}$ with $Re = \frac{UL\rho}{\mu}$ the Reynolds number defined with a flow-typical turbulent length scale L and velocity scale U. The storage requirement inhibits the applicability of DNS to three-dimensional turbulent combustion problems. The great value of DNS simulations is that they describe the real physics of turbulence. With the detailed information obtained from DNS simulations, turbulence models can be evaluated and their model constants determined.

2.2 Definition of the Reynolds- and Favre-average

Measurements of flow quantities in turbulent flows show that these quantities are strongly fluctuating in time and space. Figure 2.1 for example, shows the time history $U_1(t)$ of the axial velocity component measured on the centerline of a turbulent jet.

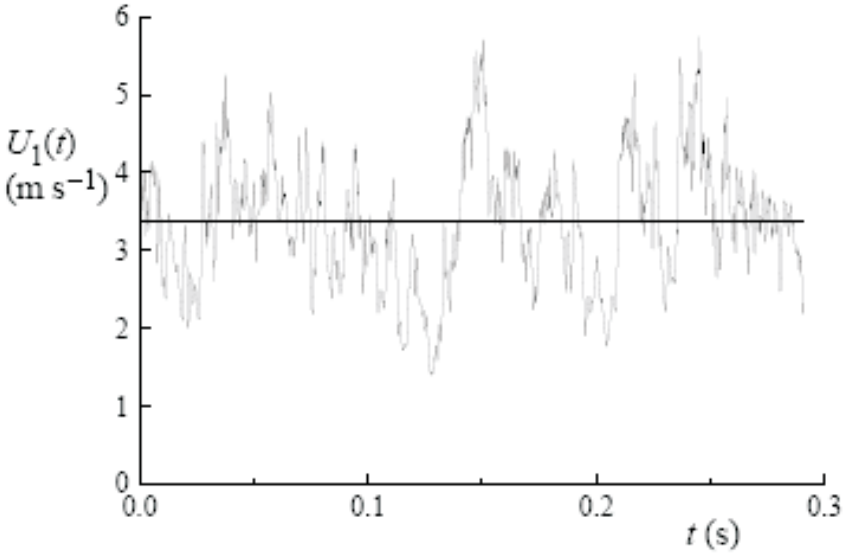

Figure 2.1: Time history of the axial velocity component $U_1(t)$ on the centerline of a turbulent jet.

Furthermore, if the experiment is repeated under the same conditions and the same measurements are performed one will obtain a different time history though the mean value will be the same. This shows that there is some kind of randomness in turbulent flows. The Navier-Stokes equations are a set of coupled, non-linear partial differential equations. The nonlinearity causes solutions to be extremely sensitive to small changes in the initial and boundary conditions. Smallest differences in the initial conditions e.g., are leading to big differences in the solutions after a short time. When we repeat an experiment, we cannot avoid small changes in the initial conditions. These small and unknown differences in the initial conditions are the reason for the different instantaneous experimental results. Therefore, flow quantities such as velocity, pressure and density are random variables which means

that we cannot predict a particular value for e.g. the instantaneous velocity U at a particular point.

A random variable such as the velocity field $\mathbf{U}(\mathbf{x},t)$ can be decomposed into its average $\langle\mathbf{U}(\mathbf{x},t)\rangle$ and its fluctuation $\mathbf{u}^{'}(\mathbf{x},t)$,

$$\mathbf{U}(\mathbf{x},t) = \langle\mathbf{U}(\mathbf{x},t)\rangle + \mathbf{u}^{'}(\mathbf{x},t) \tag{2.10}$$

The ensemble average (or Reynolds average) is defined as

$$\langle\mathbf{U}(\mathbf{x},t)\rangle = \frac{1}{N}\sum_{i=1}^{N}\mathbf{U}^{(i)}(\mathbf{x},t), \tag{2.11}$$

where N is the number of samples. The $\mathbf{U}^{(i)}(\mathbf{x},t)$ can be seen as velocity fields measured in different realizations of a turbulent flow experiment. By applying (2.11) to (2.10) one finds $\langle\mathbf{u}^{'}(\mathbf{x},t)\rangle = 0$.

In most technical applications only the mean flow quantities are of interest. To obtain equations for the mean flow quantities, one has to average the governing flow equations. In turbulent flames, density can vary by a factor of five or more. Therefore, to simplify the equations describing variable density flow it is common to use density-weighted averaging or Favre averaging to avoid explicit density correlations. Details on Favre averaging and the Favre averaged equations can be found in FRIEDRICH (1999). Favre averages are defined by:

$$\tilde{Q} = \frac{\langle\rho Q\rangle}{\langle\rho\rangle} = \frac{\frac{1}{N}\sum_{i=1}^{N}\rho^{(i)}Q^{(i)}}{\frac{1}{N}\sum_{i=1}^{N}\rho^{(i)}} \tag{2.12}$$

and Favre-decomposition into mean and fluctuation is defined as:

$$Q = \tilde{Q} + Q^{''} \tag{2.13}$$

in which $Q^{''}$ denotes the Favre-fluctuation. Note that with the definition of Favre- and Reynolds averages and fluctuations:

$$\widetilde{Q^{''}} = 0 \quad \overline{Q^{'}} = 0$$

and in general:

$$\widetilde{Q^{'}} \neq 0 \quad \overline{Q^{''}} \neq 0$$

2.3 Favre-averaged equations

Defining the Favre-averaged material derivative

$$\frac{D}{Dt} = \frac{\partial}{\partial t} + \widetilde{U}_i \frac{\partial}{\partial x_i} \tag{2.14}$$

and Favre-averaging of the continuity, momentum and scalar equations (2.1), (2.2) and (2.9) leads to:

$$\frac{D\langle\rho\rangle}{Dt} + \langle\rho\rangle \frac{\partial \widetilde{U}_i}{\partial x_i} = 0, \tag{2.15}$$

$$\langle\rho\rangle \frac{D}{Dt}\widetilde{U_j} = -\frac{\partial\langle p\rangle}{\partial x_j} + \frac{\partial\langle\tau_{ij}\rangle}{\partial x_i} + \langle\rho\rangle g_j + \frac{\partial}{\partial x_i}\langle\rho\rangle\widetilde{u_j'' u_i''}, \tag{2.16}$$

$$\langle\rho\rangle \frac{D}{Dt}\widetilde{\phi_\alpha} = -\frac{\partial}{\partial x_i}\langle J_i^\alpha\rangle + \langle\rho\rangle\widetilde{S_\alpha} - \frac{\partial}{\partial x_j}\langle\rho\rangle\widetilde{u_j'' \phi_\alpha''}, \quad \alpha = 1, 2, ...n_c. \tag{2.17}$$

Equations (2.15) and (2.16) together are referred to as Reynolds Averaged Navier-Stokes Equations (RANS-equations), although Favre-averaging was applied. The last terms on the right hand sides (RHS) represent turbulent fluxes which occur in unclosed form, since the fluctuations are unknown. The unclosed term $\langle\rho\rangle\widetilde{u_j'' u_i''}$ is called Reynolds stress tensor and the unclosed term $\langle\rho\rangle\widetilde{u_j'' \phi_\alpha''}$ is called turbulent scalar flux (see section 2.4). Another unclosed term is the averaged reaction term in equation (2.17). The accuracy of the averaged equations strongly depends on the models which are needed to close these terms. A brief introduction into closure methods for the unclosed turbulent fluxes is given in the next section and the problems of closure models for the averaged reaction rate $\widetilde{S_\alpha}$ are discussed in section 2.5.

Although some terms in the RANS equations have to be modelled, these equations are the basic equations which are solved numerically in almost all simulations of non-reactive turbulent flows of technical interest. The reason is that the discretization, necessary for a numerical solution, in space and time can be much coarser than in DNS simulations. This can be explained with the Ergodic theorem (HEINZ (2003b)). This theorem shows that taking the ensemble average of a flow variable corresponds to a spatial box-filtering of this variable. The filter width of the box is

large compared to the size of a typical turbulent eddy. The RANS equations resolve physical effects which have length scales larger than the spatial filter width, thus, they cannot describe the dynamics of the typical turbulent eddies and they need a turbulence model to be closed.

All the closure-models for the Reynolds stress and scalar fluxes are using empirical input in form of model constants. These constants are obtained from certain experiments or DNS simulations and are exactly valid just for the flows realized in those experiments and simulations. The turbulence models are not universal, their model constants have to be adapted to the flow problem under consideration. This fact reduces the predictive power of the RANS equations.

2.4 Turbulence modelling

The aim of a turbulence model is to express the unknown turbulent fluxes $\langle\rho\rangle\widetilde{u_j''u_i''}$ and $\langle\rho\rangle\widetilde{u_j''\phi_\alpha''}$ in terms of known mean quantities such as $\tilde{U}_i$ and $\tilde{\phi}_\alpha$. A common approach to close the averaged flow equations is by the standard $k-\epsilon$ model of LAUNDER and SPALDING (1972). In laminar flows energy dissipation and transport of mass, momentum and scalars normal to the streamlines is mediated by the viscosity. From experiments it is known that these transport processes are even stronger in turbulent flows. So it is natural that the effect of turbulence can be represented as an increased viscosity. This leads to the eddy-viscosity model for the Reynolds stress:

$$-\langle\rho\rangle\widetilde{u_j''u_i''} = \mu_t\left(\frac{\partial\tilde{U}_i}{\partial x_j}+\frac{\partial\tilde{U}_j}{\partial x_i}\right)-\frac{2}{3}\delta_{ij}\left(\langle\rho\rangle k+\mu_t\frac{\partial\tilde{U}_k}{\partial x_k}\right) \tag{2.18}$$

and the eddy-diffusion model for the scalars:

$$-\langle\rho\rangle\widetilde{u_j''\phi_\alpha''} = \frac{\mu_t}{\sigma_\phi}\left(\frac{\partial\tilde{\phi}_\alpha}{\partial x_j}\right) \tag{2.19}$$

in which μ_t is the turbulent or eddy viscosity and σ_ϕ is the effective Prandtl or Schmidt number for the scalar ϕ_α. In equation (2.18), k denotes the turbulent kinetic energy and is defined as:

$$k = \frac{1}{2}\widetilde{u_i''u_i''}. \tag{2.20}$$

The eddy diffusivity is derived from a single characteristic eddy length scale and a velocity scale. To find these scales, the assumption of so-called equilibrium turbulent flows is made in which the rates of production and destruction of turbulence are in near-balance. At high Reynolds numbers, there is a cascade of energy from the largest scales to the smallest ones in which the energy is dissipated. The turbulent dissipation ϵ is defined as:

$$\epsilon = \nu \widetilde{\frac{\partial u_i''}{\partial x_j} \frac{\partial u_i''}{\partial x_j}}. \tag{2.21}$$

Note that k and ϵ are defined in terms of Favre averages but that the tilde (as in $\tilde{k}$ and $\tilde{\epsilon}$) is omitted here. Assuming the turbulent spectrum to be in equilibrium, the dynamics are only governed by the energy at the large scales and the rate at which energy is transferred to the smallest, dissipative viscous scales. This leads to the following definition of the eddy viscosity:

$$\mu_t = C_\mu \langle \rho \rangle \frac{k^2}{\epsilon}, \tag{2.22}$$

in which C_μ is a model constant. To determine the remaining two unknowns k and ϵ, two transport equations have to be solved. These transport equations can be derived through standard techniques from equations (2.2) and (2.16). Modelling of these equations can be found for example in FERZIGER and PERIC (2002). The modelled k-ϵ equations read:

$$\langle \rho \rangle \frac{D}{Dt} k = \frac{\partial}{\partial x_j} \left[\left(\langle \mu \rangle + \frac{\mu_t}{\sigma_k} \right) \frac{\partial k}{\partial x_j} \right] + P_k - \langle \rho \rangle \epsilon \tag{2.23}$$

$$\langle \rho \rangle \frac{D}{Dt} \epsilon = \frac{\partial}{\partial x_j} \left[\left(\langle \mu \rangle + \frac{\mu_t}{\sigma_k} \right) \frac{\partial \epsilon}{\partial x_j} \right] + \frac{\epsilon}{k} \left(C_{\epsilon 1} P_k - C_{\epsilon 2} \langle \rho \rangle \epsilon \right) \tag{2.24}$$

with P_k the production of turbulent kinetic energy by mean shear given by:

$$P_k = -\langle \rho \rangle \widetilde{u_i'' u_j''} \frac{\partial \tilde{U}_i}{\partial x_j}. \tag{2.25}$$

Deriving the modelled equation for the viscous dissipation, the assumption has been made that production and dissipation of ϵ are proportional to respectively the production and dissipation of k.

In the modelled equations, several constants appear which have to be determined by comparison of simulations with experiments. To avoid the well known problems

of the standard $k-\epsilon$ model in round jets, a modified model, the so-called realizable $k-\epsilon$ model of FLUENT has been used. Details of this model can be found in FLUENT (2005) and SHIH et al. (1995). The model constants are presented in section 7.1.

2.5 Closure Problems of the RANS equations for turbulent reacting flows

For turbulent non-reacting flows solving the RANS equations (2.15) and (2.16), and (2.17) together with a turbulence model like the k-ϵ model gives reasonable results for many turbulent flows. However, for turbulent reacting flows these equations are yet unclosed. The problem is the term of the averaged reaction rate $\langle\rho\rangle\widetilde{S_\alpha}$ in equation (2.17) for the n_s species. This term describes the change of the mass fraction of a species due to chemical reaction. Since this term is a nonlinear function of the species and the temperature it cannot be expressed by the mean values of these scalars alone. For a simple, one-step reaction in which a fuel species reacts to product species, the chemical source term can be expressed as

$$S = A\, e^{-\frac{E_A}{R_0 T}}\, Y_F^{n_1}\, Y_O^{n_2}, \tag{2.26}$$

A is a constant, E_A is the activation energy of the reaction, T is the temperature and Y_F and Y_O are the mass fractions of the fuel and oxidizer species, respectively. The values of the exponents n_1 and n_2 are depending on the reaction under consideration. The averaged reaction rate expressed in terms of mean values and fluctuations reads

$$\widetilde{\tilde{S} = A\, e^{-\frac{E_A}{R_0(\langle T\rangle + T'')}}\, (\langle Y_F\rangle + Y_F'')^{n_1}\, (\langle Y_O\rangle + Y_O'')^{n_2}}. \tag{2.27}$$

It can be easily seen that many terms of the resulting expression contain the unknown fluctuations of temperature and mass fractions. The only possibility to close the averaged reaction rate in terms of **mean scalar values** is by assuming very fast chemical reactions. For infinitely fast reactions, the averaged reaction rate can be closed in terms of mean scalar values, but this assumption is a drastic simplification in almost all combustion processes. To close the average reaction rate term without simplifications, information on the scalar fluctuations is needed. As described in

section 2.2, the flow quantities ρ, U_i and the scalars ϕ_α are random variables. They can be described using the concepts of probability and statistics. The definition of random variables as well as the basic concepts of probability theory can be found in many textbooks e.g POPE (2003) or KLOEDEN and PLATEN (1999) and will not be repeated in this thesis. A random variable is fully described by its probability density function (PDF). The PDF of a single random variable, e.g a scalar ϕ can be defined in terms of the ensemble average:

$$f_\phi(\psi) = \langle \delta(\psi - \phi) \rangle, \tag{2.28}$$

in which ψ denotes the sample space variable associated to ϕ and δ is the Dirac-Delta distribution. The extension to more than one random variable, the so-called joint PDF for the n_c scalars, reads:

$$f_\phi(\boldsymbol{\psi}) = \left\langle \prod_{\alpha=1}^{n_c} \delta(\psi_\alpha - \phi_\alpha \right\rangle \tag{2.29}$$

where $\boldsymbol{\psi} = (\psi_1, ..., \psi_{n_s})$ is the sample space vector associated to the vector of scalars $\boldsymbol{\phi}$. It can be seen from (2.26), that the reaction rate is a function of the n_s mass fractions and temperature. If the joint PDF for the scalars is known, the averaged reaction rate can be obtained by,

$$\tilde{S}(\boldsymbol{\phi}) = \frac{1}{\langle \rho \rangle} \int_\psi S(\boldsymbol{\psi}) \rho(\psi) f_\phi(\boldsymbol{\psi}) d\boldsymbol{\psi}. \tag{2.30}$$

This expression is closed, because the joint scalar PDF contains the necessary information of the scalar fluctuations.

As shown above, the knowledge of the joint scalar PDF could close the averaged reaction term. To calculate the PDF, a transport equation for this PDF has to be derived and solved. The transport equation for the joint PDF is presented in chapter 3.2 and a numerical tractable solution method is presented in section 3.3.

Chapter 3

Stochastic modelling of turbulent reactive flows (PDF equations)

To avoid the closure problems of the averaged reaction rate, a transport equation for the joint velocity composition PDF can be used to describe turbulent reactive flows. The joint velocity composition PDF contains the information on the combined statistics of velocity and scalars, thus completely determining the flow and scalar fields of turbulent reactive flows. Unfortunately, the numerical solution of the transport equation for the joint velocity composition PDF is computationally expensive and likely to become unstable. A numerically more efficient and robust approach is, to solve the RANS equation together with a turbulence model for the flow field and a transport equation only for the joint scalar PDF to include the exact chemistry. This is called the hybrid solution approach.

In the first section of this chapter, the transport equation for the joint velocity composition PDF is presented. The transport equation for the joint composition PDF is presented in section 3.2. The last section presents a numerical solution method for the joint composition PDF transport equation.

3.1 Transport equation for the joint velocity composition PDF

Since the velocity and scalar fluctuations are not independent in a turbulent flow field, the transport equation for the one-point joint velocity-scalar PDF $f_{U\phi}(\mathbf{V}, \boldsymbol{\psi}; \mathbf{x}, t)$ is presented in this chapter. From the definition of a PDF follows that $f_{U\phi}(\mathbf{V}, \boldsymbol{\psi}; \mathbf{x}, t) d\mathbf{V} d\boldsymbol{\psi}$ is the probability that the velocity is in the interval $[\mathbf{V}, \mathbf{V} + d\mathbf{V})$ **and** the scalar variables are in the interval $[\boldsymbol{\psi}, \boldsymbol{\psi} + d\boldsymbol{\psi})$ at $(\mathbf{x}, t)$.

$$f_{U\phi}(\mathbf{V}, \boldsymbol{\psi}; \mathbf{x}, t) d\mathbf{V} d\boldsymbol{\psi} = P\left[\{V_i \leq U_i < V_i + dV_i\} \bigcap \{\psi_\alpha \leq \phi_\alpha < \psi_\alpha + d\psi_\alpha\}\right] \quad (3.1)$$

For variable density flows , it is useful to consider the joint mass density function (MDF),

$$F_{U\phi}(\mathbf{V}, \boldsymbol{\psi}, \mathbf{x}; t) = \rho(\boldsymbol{\psi}) f_{U\phi}(\mathbf{V}, \boldsymbol{\psi}; \mathbf{x}, t). \tag{3.2}$$

$F_{U\phi}(\mathbf{V}, \boldsymbol{\psi}, \mathbf{x}; t)$ gives the expected density of mass with velocity $\mathbf{V}$ and composition $\boldsymbol{\psi}$ at position $\mathbf{x}$.

$$\int_{\mathbf{V}} \int_{\boldsymbol{\psi}} F_{U\phi}(\mathbf{V}, \boldsymbol{\psi}, \boldsymbol{x}; t) d\mathbf{V} d\boldsymbol{\psi} = \langle \rho(\boldsymbol{x}, t) \rangle. \tag{3.3}$$

The Favre average of an arbitrary function $Q(\boldsymbol{U}, \boldsymbol{\phi})$ can be considered in terms of the MDF:

$$\tilde{Q}(\mathbf{U}, \boldsymbol{\phi}) = \int_{V,\psi} Q(\mathbf{V}, \boldsymbol{\psi}) F_{U\phi}(\mathbf{V}, \boldsymbol{\psi}) d\mathbf{V} d\boldsymbol{\psi}. \tag{3.4}$$

From the Navier Stokes equations (2.1)-(2.2) and the scalar transport equation (2.9) the MDF transport equation can be expressed as:

$$\begin{aligned} \frac{\partial F_{U\phi}}{\partial t} & + V_j \frac{\partial F_{U\phi}}{\partial x_j} + \left(-\frac{1}{\rho(\boldsymbol{\psi})} \frac{\partial \langle p \rangle}{\partial x_i} + \frac{1}{\rho(\boldsymbol{\psi})} \frac{\partial \langle \tau_{ij} \rangle}{\partial x_j} + g_i \right) \frac{\partial F_{U\phi}}{\partial V_i} \\ & + \frac{\partial}{\partial \psi_\alpha} S_\alpha(\boldsymbol{\psi}) F_{U\phi} \\ & = \frac{\partial}{\partial V_i} \left[\frac{1}{\rho(\boldsymbol{\psi})} \left\langle \left(\frac{\partial p'}{\partial x_i} - \frac{\partial \tau'_{ij}}{\partial x_j} \right) | \mathbf{V}, \boldsymbol{\psi} \right\rangle F_{U\phi} \right] \\ & - \frac{\partial}{\partial \psi_\alpha} \left[\frac{1}{\rho(\boldsymbol{\psi})} \left\langle -\frac{\partial J_j^{\alpha'}}{\partial x_j} | \mathbf{V}, \boldsymbol{\psi} \right\rangle F_{U\phi} \right] \end{aligned} \tag{3.5}$$

A detailed derivation of this equation can be found in POPE (1985). The terms of the left-hand side (LHS) are in closed form, i.e. the MDF $F_{U\phi}$, once known, provides the information necessary to evaluate these terms. The first term on the LHS describes the evolution of probability with time. The second term represents the convection of probability in physical space. In the third term, transport in velocity space is expressed. This transport is due to the mean pressure gradient, the mean viscous stress tensor gradient and gravity. For the further approach, the mean viscous stress tensor gradient is neglected under the assumption of high Reynolds numbers. The last term on the LHS contains the chemical source terms. The reaction rates are determined by the thermochemical scalars $\boldsymbol{\phi}$. The MDF contains the full information of the scalar statistics, therefore the chemical source term occurs in closed form in this transport equation. The fact that reactions can be treated

exactly for arbitrary complex chemical kinetics is one of the main reasons for using the PDF formulation in turbulent reactive flows.

The two terms on the RHS of the transport equation contain means of gradients of quantities conditional on the values of velocity and composition. The one-point one-time joint velocity scalar mass density function $F_{U\phi}(\mathbf{V}, \boldsymbol{\psi}, \mathbf{x}; t)$ does not provide information on gradient statistics and therefore these terms occur in unclosed form and have to be modelled. Note that gradients of unconditional means do not present closure problems, since these means are known at all positions in physical space. The first unclosed term on the RHS describes transport of probability in velocity space induced by the fluctuating viscous stresses and the fluctuating pressure gradient. The second term represents transport in composition space by molecular fluxes. Closure models for the terms on the RHS can be found in WOUTERS (1998) or FOX (2003).

As described in section 3.3, the FLUENT package uses a hybrid approach to calculate turbulent reactive flows. This means that a conventional finite volume solver is used to calculate the turbulent flow field. For the scalar composition, a stochastic model is applied and these two submodels are connected by the fluid density. It turned out (FOX (2003)) that this hybrid approach is numerically more efficient and stable than solving the joint velocity composition PDF. Therefore, a transport equation for the joint composition PDF $f_\phi(\boldsymbol{\psi}; \mathbf{x}, t)$ has to be derived. This procedure is presented in the next section.

3.2 Transport equation for the joint composition PDF

The one-point one-time joint composition PDF is the marginal of the joint velocity scalar PDF and can be obtained by integrating over the velocity space. Equivalently, the joint Composition Mass Density Function (CMDF) is obtained by integration of the MDF,

$$F_\phi(\boldsymbol{\psi}, \mathbf{x}; t) = \int_V F_{U\phi}(\mathbf{V}, \boldsymbol{\psi}, \mathbf{x}; t) d\mathbf{V}. \tag{3.6}$$

Analogously, the transport equation for CMDF is obtained by integrating (3.5)

over the velocity space. On obtains:

$$\begin{aligned}\frac{\partial F_\phi}{\partial t} \quad & +\widetilde{U}_j \frac{\partial F_\phi}{\partial x_j} + \frac{\partial}{\partial \psi_\alpha} S_\alpha(\boldsymbol{\psi}) F_\phi \\ & = -\frac{1}{\langle\rho\rangle}\frac{\partial}{\partial x_i}\left[\langle\rho\rangle\langle u_i^{''}|\boldsymbol{\psi}\rangle F_\phi\right] - \frac{\partial}{\partial \psi_\alpha}\left[\frac{1}{\rho(\boldsymbol{\psi})}\left\langle -\frac{\partial J_j^{\alpha'}}{\partial x_j}|\boldsymbol{\psi}\right\rangle \; F_\phi\right].\end{aligned} \tag{3.7}$$

The terms one the LHS appear in closed form and describe evolution of probability in time, convection of probability in the physical space with the mean velocity and transport in composition space due to chemical reaction respectively. Terms on the RHS are unclosed. The first term represents the turbulent transport of probability in physical space (turbulent scalar flux), the second term describes the transport of probability in composition space due to molecular fluxes and is further referred to as micro-mixing term.

Using appropriate models to close these two terms, one would be able to solve the transport equation (3.7) by using standard discretization methods such as finite differences or finite-volume. A typical combustion problem involves more than ten species ($n_s = 10$), therefore $n_c = 11$. Assuming a steady state, three-dimensional problem the dimension of $F_\phi(\boldsymbol{\psi}, \mathbf{x})$ is $n = n_c{+}3 = 14$. Since the memory requirement of finite-volume and finite-difference schemes increases roughly exponentially with dimensionality, they are not very attractive for these high dimensional problems. A numerically tractable solution method for equation (3.7) and closure models for the two unclosed terms are presented in the next sections.

3.3 Monte Carlo Method

3.3.1 Particle representation of the CMDF

A good way to understand the particle representation of a PDF, is by considering a turbulent reactive flow experiment in which one measures for example the n_s species mass fractions and the enthalpy in the domain of interest. Repeating the experiment N times will lead to N different results for the composition vector $\boldsymbol{\phi}^{(1)}...\boldsymbol{\phi}^{(N)}$, since the turbulent flow is a stochastic process (see section 2.2). Each realization of the experiment is called a particle. Using the definition of the PDF in terms of the

ensemble average,

$$f_\phi(\boldsymbol{\psi}) = \frac{1}{N}\sum_{i=1}^{N}\prod_{\alpha=1}^{n_c}\delta(\psi_\alpha - \phi_\alpha^{(i)}) \tag{3.8}$$

the PDF can be calculated. This PDF is not the "exact PDF", it is more an estimate of the exact PDF. It can be seen as a discrete representation of the exact PDF. The more experimental results (particles) are available, the better is the estimate. Mathematically, as $N \to \infty$, the exact PDF is obtained. As it was shown in section 2.5, the purpose of PDF's is to calculate the mean or variance of a function $Q(\boldsymbol{\phi})$:

$$\langle Q(\boldsymbol{\phi})\rangle = \int_{-\infty}^{\infty} f_\phi(\boldsymbol{\psi})Q(\boldsymbol{\psi})d\boldsymbol{\psi} = \frac{1}{N}\sum_{i=1}^{N} Q(\boldsymbol{\phi}^{(i)}) \tag{3.9}$$

To compare the quality of the estimate PDF with the exact PDF, the statistical error ϵ_{QN} is defined:

$$\epsilon_{QN} = \langle Q\rangle_N - \langle Q\rangle_{N\to\infty} \tag{3.10}$$

For large N, the standard deviation $\sigma_{\epsilon_{QN}}$ (square root of the variance) of ϵ_{QN} is

$$\sigma_{\epsilon_{QN}} = \frac{1}{\sqrt{N}}\sigma_Q. \tag{3.11}$$

as it can be found in NOOREN (1998). Thus, the statistical error decreases as $\frac{1}{\sqrt{N}}$. For the particle (or discrete) representation of a PDF it is not important if the particles (or samples) $\boldsymbol{\phi}^{(1)}...\boldsymbol{\phi}^{(N)}$ are obtained from different realizations of a particular flow experiment or if they are obtained numerically. The way how the particles can be obtained numerically is explained in section 3.3.2.

The particles used in the representation of the CMDF have the properties composition $\boldsymbol{\phi}^{(i)}$ and position $\mathbf{x}^{(i)}$. F_ϕ is closely related to the mean density in the flow:

$$\int_\psi F_\phi(\boldsymbol{\psi}, \boldsymbol{x}; t)d\boldsymbol{\psi} = \langle\rho(\boldsymbol{x}, t)\rangle. \tag{3.12}$$

To obtain the correct discrete representation of the CMDF, it is necessary to associate a mass with each of the particles. Consider a turbulent reactive flow in a Volume V. The expected total mass M of the mixture in V is

$$M = \int_V \langle\rho(\boldsymbol{x})\rangle dV \tag{3.13}$$

If the CMDF is represented by N particles, then the mass Δm associated with each particle is

$$\Delta m = \frac{M}{N}. \tag{3.14}$$

The discrete CMDF F_ϕ is now written as

$$F_\phi(\boldsymbol{\psi}, \boldsymbol{x}; t) = \Delta m \sum_{i=1}^{N} \delta(\boldsymbol{\psi} - \boldsymbol{\phi}^{(i)}) \delta(\boldsymbol{x} - \boldsymbol{x}^{(i)}). \tag{3.15}$$

Here, $\delta(\boldsymbol{\psi} - \boldsymbol{\phi}^{(i)})$ is a short notation for $\prod_{\alpha=1}^{n_c} \delta(\psi_\alpha - \phi_\alpha^{(i)})$. Integration of the relation (3.15) over the entire $\boldsymbol{\psi} - \mathbf{x}$ space and taking the mean gives the desired expression for the expected total mass M in V.

3.3.2 Relationship between PDF transport equations and stochastic differential equations

As shown in the last section, constructing a discrete representation of the CMDF is possible if an ensemble of realizations of a turbulent flow (particles) is known. The purpose of this section is to present a stochastic description for the particles and to show the relationship between the PDF transport equation and the stochastic evolution equation for the particles. The description given in this section is very brief. A detailed derivation of the results presented here can be found in HEINZ (2003b) and FOX (2003) and the references therein.

As described in section 2.2, the quantities of a turbulent flow such as velocity $\boldsymbol{U}$ and scalars $\boldsymbol{\phi}$ are random variables that depend on $(\boldsymbol{x}, t)$. Instead of using this Eulerian coordinate description, we consider now the Lagrangian coordinate equivalent for a so-called notional particle. In the Eulerian PDF context, a notional particle serves only as a discrete representation of the Eulerian PDF and not as a model for a real Lagrangian fluid particle. A Lagrangian notional particle follows a trajectory in velocity-composition-physical space (i.e., $\boldsymbol{U}^*(t), \boldsymbol{\phi}^*(t), \boldsymbol{X}^*(t)$) starting from a random location $\boldsymbol{Y}$ in the physical domain:

$$\begin{aligned} \boldsymbol{U}^*(0) &= \boldsymbol{U}(\boldsymbol{Y}, t_0), \\ \boldsymbol{\phi}^*(0) &= \boldsymbol{\phi}(\boldsymbol{Y}, t_0), \\ \boldsymbol{X}^*(0) &= \boldsymbol{Y}. \end{aligned} \tag{3.16}$$

where t_0 is an arbitrary fixed reference time and $\boldsymbol{U}(\boldsymbol{x},t)$ and $\boldsymbol{\phi}(\boldsymbol{x},t)$ are the Eulerian velocity and composition fields, respectively. Note that, even though $\boldsymbol{Y}$ and t_0 are fixed, the initial velocity and composition will be random variables, since $\boldsymbol{U}(\boldsymbol{x},t)$ and $\boldsymbol{\phi}(\boldsymbol{x},t)$ are random fields. A notional-particle trajectory is defined by stochastic differential equations (SDE's) of the form:

$$\frac{d\boldsymbol{X}^*}{dt}(t) = \boldsymbol{U}^*(t) \tag{3.17}$$

$$d\boldsymbol{U}^*(t) = \boldsymbol{a}_U(\boldsymbol{U}^*(t),\boldsymbol{\phi}^*(t),\boldsymbol{X}^*(t),t)dt + \boldsymbol{B}_U(\boldsymbol{U}^*(t),\boldsymbol{\phi}^*(t),\boldsymbol{X}^*(t),t)d\boldsymbol{W}(t) \tag{3.18}$$

$$d\boldsymbol{\phi}^*(t) = \boldsymbol{a}_\phi(\boldsymbol{U}^*(t),\boldsymbol{\phi}^*(t),\boldsymbol{X}^*(t),t)dt + \boldsymbol{B}_\phi(\boldsymbol{U}^*(t),\boldsymbol{\phi}^*(t),\boldsymbol{X}^*(t),t)d\boldsymbol{W}(t) \tag{3.19}$$

in which $\boldsymbol{a}_U, \boldsymbol{a}_\phi$ are the drift coefficients and $\boldsymbol{B}_U, \boldsymbol{B}_\phi$ are the diffusion coefficients. The expression $d\boldsymbol{W}(t)$ is the increment of a vectorial Wiener process and is determined by:

$$\langle d\boldsymbol{W}(t)\rangle = 0 \tag{3.20}$$

and

$$\langle dW_i(t)dW_j(t)\rangle = dt\delta_{ij}. \tag{3.21}$$

Since $\boldsymbol{X}^*(t)$,$\boldsymbol{U}^*(t)$ and $\boldsymbol{\phi}^*(t)$ are stochastic processes (random variables which depend on time), they can be fully described by their Lagrangian PDF which is conditioned on the initial location:

$$f_L^* \equiv f_{\boldsymbol{U}^*,\boldsymbol{\phi}^*,\boldsymbol{X}^*|\boldsymbol{Y}}(\boldsymbol{V},\boldsymbol{\psi},\boldsymbol{x} \mid \boldsymbol{y};t). \tag{3.22}$$

This conditional PDF is governed by the corresponding Fokker-Planck equation:

$$\frac{\partial f_L^*}{\partial t} + V_i\frac{\partial f_L^*}{\partial x_i} + \frac{\partial}{\partial z_i}[a_i(\boldsymbol{z},\boldsymbol{x},t)f_L^*] = \frac{1}{2}\frac{\partial^2}{\partial z_i \partial z_j}[b_{ij}(\boldsymbol{z},\boldsymbol{x},t)f_L^*], \tag{3.23}$$

where $\boldsymbol{z} = [\boldsymbol{V}\ \boldsymbol{\psi}]^T$, $\boldsymbol{a}(\boldsymbol{z},\boldsymbol{x},t) = [\boldsymbol{a}_U\ \boldsymbol{a}_\phi]^T$ and the diffusion matrix $\boldsymbol{B} = [b_{ij}]$ is given by

$$\boldsymbol{B}(\boldsymbol{z},\boldsymbol{x},t) = \begin{pmatrix} \boldsymbol{B}_U\boldsymbol{B}_U^T & \boldsymbol{0} \\ \boldsymbol{0} & \boldsymbol{B}_\phi\boldsymbol{B}_\phi^T) \end{pmatrix}. \tag{3.24}$$

Since the PDF transport equation is known (see section 3.2), the drift and diffusion terms can be determined. The transport equation for the PDF f_L^* can therefore be solved by solving the SDE's (3.17)-(3.19) for many different notional particles with different $\boldsymbol{Y}$. Numerical solution methods for SDE can be found in KLOEDEN

and PLATEN (1999). For example, equation (3.19) can be solved numerically by using the Euler scheme for SDE's:

$$\begin{array}{l}\boldsymbol{\phi}^*(t+\Delta t) = \boldsymbol{\phi}^*(t) + \boldsymbol{a}_\phi(\boldsymbol{U}^*(t), \boldsymbol{\phi}^*(t), \boldsymbol{X}^*(t), t)\Delta t \\ +\boldsymbol{B}_\phi(\boldsymbol{U}^*(t), \boldsymbol{\phi}^*(t), \boldsymbol{X}^*(t), t)\,(\boldsymbol{W}(t+\Delta t) - \boldsymbol{W}(t))\end{array} \tag{3.25}$$

In the same way, starting with the transport equation for the CMDF (3.7) a corresponding SDE can be found that describes the evolution of notional particles. The CMDF can then be obtained by equation (3.15). The problem of solving a high dimensional transport equation is reduced to solve a system of SDE's for N particles. The more particles are considered, the more accurate is the solution. It can be shown, that the memory requirement depends only linearly on the problem's dimensionality. In the next section, models for the unclosed terms in the CMDF transport equation are presented.

3.4 Closure models for the turbulent scalar flux and the micro-mixing

The turbulent scalar flux $-\frac{1}{\langle\rho\rangle}\frac{\partial}{\partial x_i}\left[\langle\rho\rangle\langle u_i''|\boldsymbol{\psi}\rangle F_\phi\right]$ in (3.7) is unclosed, because the velocity fluctuations are unknown in the joint composition mass density formulation. The turbulent scalar flux is modelled by the gradient diffusion assumption

$$-\frac{1}{\langle\rho\rangle}\frac{\partial}{\partial x_i}\left[\langle\rho\rangle\langle u_i''|\boldsymbol{\psi}\rangle F_\phi\right] = -\frac{1}{\langle\rho\rangle}\frac{\partial}{\partial x_i}\left(\frac{\mu_t}{\rho Sc_t}\frac{\partial F_\phi}{\partial x_i}\right), \tag{3.26}$$

where μ_t is the turbulent viscosity and Sc_t is the turbulent Schmidt number, defined as:

$$Sc_t = \frac{\nu_t}{\Gamma_t}. \tag{3.27}$$

Γ_t is the turbulent diffusivity, $\Gamma_t \propto \frac{k^2}{\epsilon}$. The turbulent viscosity μ_t is determined from the $k-\epsilon$ model as it is described in section 2.4.

The transport of probability in composition space by molecular fluxes (micro-mixing) represented by the term $\frac{\partial}{\partial\psi_\alpha}[\frac{1}{\rho(\boldsymbol{\psi})}\langle-\frac{\partial J_j^{\alpha'}}{\partial x_j}|\boldsymbol{\psi}\rangle\ F_\phi]$ is unclosed. For the simulation of turbulent flames, this term is very critical since combustion occurs at the smallest scales. Modelling of the micro-mixing is not straightforward and is the weakest link in the PDF approach. The three mixing models which are available

in FLUENT, are presented briefly. A more detailed description of the different micro-mixing models and their requirements can be found in FOX (2003).

IEM Model:

The simplest micro-mixing model is the Interaction by Exchange with the Mean (IEM) model. In this model, the scalar values of individual particles are subject to a deterministic relaxation towards the mean value:

$$d\boldsymbol{\phi}^{(i)} = \frac{1}{2} C_\phi \frac{\epsilon}{k} \left(\boldsymbol{\phi}^{(i)} - \tilde{\boldsymbol{\phi}} \right), \tag{3.28}$$

where (i) denotes a specific particle and $\tilde{\phi}$ is the Favre scalar average obtained from all particles. The scalar decay frequency is taken to be proportional to the turbulence frequency. The proportionality factor C_ϕ is not a universal constant but depends on the initial ratio between the turbulence and scalar length scales as well as on the Reynolds number. In HEINZ (2003b), a function for C_ϕ depending on the Taylor micro-scale Reynolds number is presented. The standard value for C_ϕ is 2.0.

A generalization of the IEM model was suggested recently by HEINZ (2003a). This model revealed excellent performance compared to DNS mixing data. However, it was not applied in combustion applications until now.

The Modified Curl Model:

For the modified Curl model, a few particle pairs are selected at random from all the particles in a cell. Their individual compositions are moved towards their mean composition. For the special case of equal particle mass, the number of particle pairs selected is calculated as

$$N_{pair} = \frac{1.5 C_\phi N \Delta t \epsilon}{k}, \tag{3.29}$$

where Δt is the time step and N is the total number of particles in the cell. For each particle pair, a uniform random number ξ is selected and each particle's composition $\boldsymbol{\phi}$ is moved towards the pair's mean composition by a factor proportional to ξ:

$$\begin{aligned} \boldsymbol{\phi}^i(t+\Delta t) &= (1-\xi)\boldsymbol{\phi}^{(i)}(t) + \xi \frac{\left(\boldsymbol{\phi}^{(i)}(t) m_i + \boldsymbol{\phi}^{(j)}(t) m_j \right)}{(m_i + m_j)} \\ \boldsymbol{\phi}^j(t+\Delta t) &= (1-\xi)\boldsymbol{\phi}^{(j)}(t) + \xi \frac{\left(\boldsymbol{\phi}^{(i)}(t) m_i + \boldsymbol{\phi}^{(j)}(t) m_j \right)}{(m_i + m_j)} \end{aligned} \tag{3.30}$$

where $\boldsymbol{\phi}^{(i)}$ and $\boldsymbol{\phi}^{(j)}$ are the composition vectors of particles i and j and m_i, m_j are the masses of particles i and j.

The molecular mixing occurs between neighbouring points in physical space. The scalar fields are always continuous and therefore micro-mixing is local in composition space. This localness property is obviously violated in the modified Curl and IEM models.

EMST Model:

The Euclidean Minimum Spanning Tree (EMST) model mixes particle pairs that are close to each other in composition space. The particle pairing is determined by a Euclidean Minimum Spanning Tree, which is the minimum length of the set of edges connecting one particle to at least one other particle. Details on the EMST model can be found in POPE and SUBRAMANIAM (1998).

3.5 Hybrid solution method

In Fluent, a Monte Carlo algorithm is used in combination with a conventional finite volume description of the turbulent flow field. Together, the Monte Carlo and the finite volume submodels form a so-called hybrid model. In this work, the $k-\epsilon$ turbulence model as it is described in section 2.4 is used. However, FLUENT allows also to use other turbulence models, e.g. Reynolds stress closure models. The main motivation for the use of the hybrid method is, that it combines the advantages of both methods. The hybrid algorithm is illustrated in figure 3.1 .

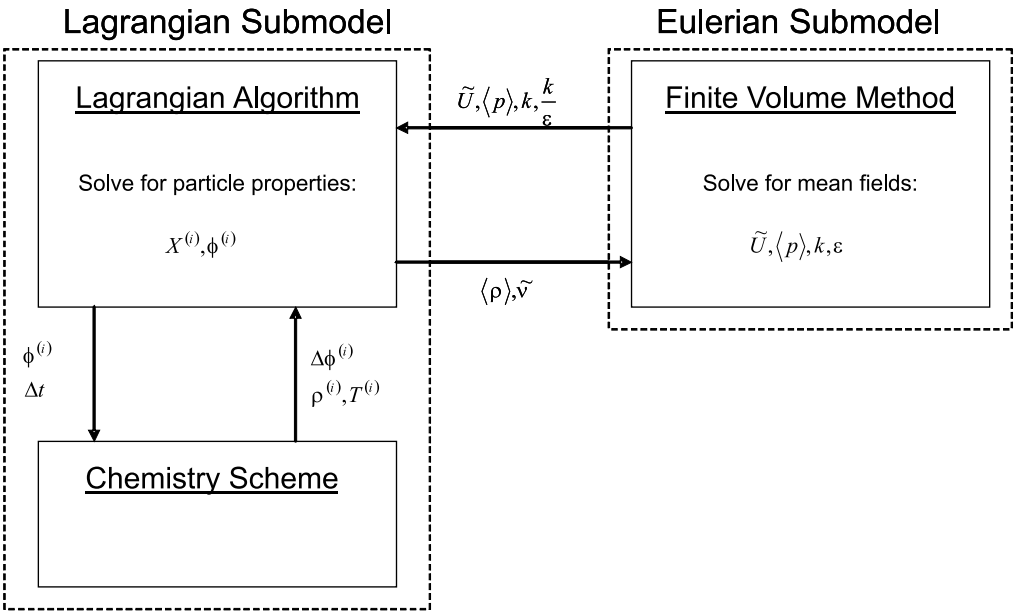

Figure 3.1: Sketch of the hybrid solver

From the finite volume turbulence submodel the mean field values and the time scale information necessary for the mixing models can be obtained. The particles used in the Monte Carlo method have the properties mass, position and composition. The mass of the particles is such that the sum of the particle masses in a cell equals the cell mass (cell volume times average density). In simulations of flows with complicated geometry, large changes in cell volumes are often unavoidable. Therefore, the particle masses are adjusted so that the number of particles in a cell is controlled to be approximately constant and uniform in all grid cells.

The finite volume submodel solves for the mean velocity $\tilde{\boldsymbol{U}}$, the turbulence kinetic energy k, the turbulent dissipation rate ϵ and the mean pressure $\langle p \rangle$. These values and the turbulent time scale $\tau_t = \frac{k}{\epsilon}$, the turbulent viscosity μ_t and the turbulent Schmidt number Sc_t are then passed to the Monte Carlo submodel. In the Monte Carlo submodel, the particles are moved through the domain by a spatially second order accurate Lagrangian method. The particles evolve due to different processes such as convection, diffusion, mixing and reaction. For the numerical solution these processes are applied in different, so-called fractional steps. In a first convection step, particles are advanced to a new position

$$\boldsymbol{X}^{(i)}\left(t+\frac{\Delta t}{2}\right) = \boldsymbol{X}^{(i)}(t) + \tilde{\boldsymbol{U}}\left(\boldsymbol{x}=\boldsymbol{X}^{(i)}(t), t\right)\frac{\Delta t}{2}, \tag{3.31}$$

where $\boldsymbol{X}^{(i)}$ is the position vector of the i-th particle and Δt is the particle time step. For unsteady flows, the particle time step is the physical time step. For steady-state flows, local time steps are calculated for each cell as

$$\Delta t = min(\Delta t_{conv}, \Delta t_{diff}, \Delta t_{mix}), \tag{3.32}$$

where

$$\begin{aligned} \Delta t_{conv} &= \frac{0.5\Delta x}{|\tilde{\boldsymbol{U}}_{cell}|}, \\ \Delta t_{diff} &= \frac{0.5(\Delta x)^2}{|\boldsymbol{\Gamma}_{\boldsymbol{t}cell}|}, \\ \Delta t_{mix} &= 0.5\tau_t \end{aligned} \tag{3.33}$$

and $\Delta x = V_{cell}^{\frac{1}{3}}$ is the characteristic cell length. The next fractional step is the mixing step. One of the models described in the previous section is applied, for example the IEM model:

$$\boldsymbol{\phi}^{(i)}\left(t+\frac{\Delta t}{2}\right) = \boldsymbol{\phi}^{(i)}(t) - \left(1-\exp\left(\frac{1}{2}C_{\phi}\frac{\epsilon}{k}\right)\right)(\boldsymbol{\phi}^{(i)}(t) - \tilde{\boldsymbol{\phi}}). \tag{3.34}$$

After the mixing step, the reaction fractional step is applied in which the chemical source term is integrated over the local time step Δt:

$$\boldsymbol{\phi}^{(i)}(t) = \boldsymbol{\phi}^{(i)}\left(t+\frac{\Delta t}{2}\right) + \int_{t}^{t+\frac{\Delta t}{2}} S(\boldsymbol{\phi}^{(i)}(s))ds \tag{3.35}$$

In practice, the integral must be evaluated using a stiff ODE solver. Because transported PDF simulations are typically used for reacting flows with complex chemistry, the chemical reaction step will often dominate the overall computational costs. A computationally affordable way to calculate the integral in (3.35) is by creating a lookup table as it is described in section 4.3. Finally, the second convection step is calculated as

$$\begin{aligned}\boldsymbol{X}^{(i)}(t) &= \boldsymbol{X}^{(i)}\left(t+\tfrac{\Delta t}{2}\right) \\ &+\Delta t\left(\tilde{\boldsymbol{U}}\left(\boldsymbol{x}=\boldsymbol{X}^{(i)}\left(t+\tfrac{\Delta t}{2}\right),\left(t+\tfrac{\Delta t}{2}\right)\right) - \frac{1}{2}\tilde{\boldsymbol{U}}(\boldsymbol{x}=\boldsymbol{X}^{(i)}(t),t)\right) \\ &+\Delta t\left(\frac{1}{\langle\rho\rangle Sc_t}\frac{\partial\mu_t}{\partial\boldsymbol{X}} + (\boldsymbol{W}(t+\Delta t)-\boldsymbol{W}(t))\sqrt{\frac{2\mu_t}{\langle\rho\rangle\Delta t Sc_t}}\right),\end{aligned} \tag{3.36}$$

where $\boldsymbol{W}(t)$ is a vectorial Wiener process. After the fractional steps are calculated for each particle in every cell, the CMDF can be obtained by equation 3.15. Once the CMDF is known, the Favre averages of the species mass fractions, the Favre average of the kinematic viscosity and the average density for each cell can be obtained. The averaged density $\langle\rho\rangle$ and the averaged viscosity $\tilde{\nu}$ are then used in the next finite volume sub-step.

Chapter 4

Chemistry models

4.1 Introduction

The big advantage of the Monte Carlo PDF formulation for turbulent reactive flows is the closed treatment of the chemical source term. In this chapter, the incorporation of chemical reaction in the Monte Carlo method is discussed. The global reaction describing the oxidation of methane, the main component of natural gas, to carbon dioxide and water is simply

$$CH_4 + 2O_2 \rightarrow CO_2 + 2H_2O.$$

However, the real combustion process is much more complicated. The conversion of methane and oxygen into combustion products includes many intermediate species participating in a large number of elementary reactions. Detailed chemical kinetic mechanisms, like the GRI-Mech 3.0 (see SMITH, GOLDEN, and FRENKLACH (SMITH et al.)) mechanism, include 53 species and 325 elementary reactions. Their performance is shown in one dimensional laminar flame calculations. The calculated results show very good agreement with experimental data. This indicates, that these detailed mechanisms provide a realistic and reliable description of the real combustion process. It would be very attractive, to incorporate detailed chemical mechanisms directly into the Monte Carlo PDF model. Using the GRI-Mech 3.0 mechanism, the composition space would be 54-dimensional. The memory and CPU resources of present day computers do not allow for an accurate representation of such a high dimensionality PDF in the Monte Carlo method. The chemical source term $S(\phi)$ describes the rate of change of the species mass fraction for every species. It consists of a coupled ODE system with the dimension n_s. In the particle reaction step (see equation (3.35), this ODE system has to be integrated for each particle in every iteration. Since the ODE system is stiff, the numerical solution is computationally very expensive. For the GRI-Mech 3.0 mechanism, 53 coupled, stiff

ODE's would have to be solved for each particle in each iteration. This presents another limit of the applicability of detailed chemical mechanisms in the Monte Carlo PDF model. Therefore, the detailed chemical mechanisms have to be reduced somehow, in order to incorporate them into the Monte Carlo PDF model. Choosing an appropriate chemical mechanism for the simulations of non-premixed turbulent flames is very important. The mechanism has to be able to describe finite rate effects such as ignition delay and local extinction. For the simulations of the Delft III flame, the mechanism additionally has to be able to describe the premixed combustion of acetylene (C_2H_2) in the pilot flames.

In the first part of this chapter, methods to reduce detailed chemical mechanisms are presented. A tabulation algorithm is also presented, which reduces the number of ODE integrations in the reaction fractional step of the Monte Carlo PDF method. This so-called ISAT (see POPE (1997)) algorithm provides speed ups in the simulations up to 100.

4.2 Skeletal chemical kinetic mechanism

Dutch natural gas consists mainly of methane(CH_4), ethane(C_2H_6) and nitrogen(N_2). The mixture contains only a small amount of higher alkanes. The composition up to hexane and two simplified compositions from NOOREN (1998) are presented in table 4.1.

component	natural gas [mol%]	$NG-C_2$ [mol%]	$NG-C_1$ [mol%]
CH_4	81.29	80.95	85.30
C_2H_6	2.87	3.89	-
C_3H_8	0.38	-	-
C_4H_{10}	0.15	-	-
C_5H_{12}	0.04	-	-
C_6H_{14}	0.05	-	-
N_2	14.32	14.26	14.70
O_2	0.01	0.01	-
CO_2	0.89	0.89	-

Table 4.1: Average composition of Dutch natural gas. $NG-C_1$ and $NG-C_2$ are two simplified compositions.

The simplified compositions have the same caloric value and stoichiometric mixture fraction as the real natural gas, but include less species. The $NG - C_1$ composition only contains C_1 species, the $NG - C_2$ contains C_1 and C_2 species and is used in this work. As described above, detailed chemical mechanisms such as the GRI-Mech 3.0 are numerically not tractable for three-dimensional simulations of a non-premixed turbulent flame. The reduction of the detailed mechanism to a so-called skeletal mechanism is done for a particular flame condition of interest. For example by applying the detailed mechanism in the calculation of a Perfectly Stirred Reactor (PSR). The model equation of the PSR can be found in CHEN (1997). By identifying and eliminating the unimportant reaction steps in the detailed mechanism, the skeletal mechanism is developed iteratively. Different criterions for the determination of unimportant reactions can be used. In this section the criterions used in CHEN (1997) are briefly presented. Let $S_k^d,\ k = 1, 2...n_s+1$ be the temperature and species composition obtained with the detailed mechanism and S_k^s be those obtained with the skeletal mechanism. Then, a criterion that has to be satisfied by the skeletal mechanism can be set as

$$\max_k \left| \frac{S_k^d - S_k^s}{S_k^d} \right| \leq \delta \tag{4.1}$$

where δ is a small number, e.g. 0.05. This number represents the relative difference in the solutions obtained with the detailed and the skeletal mechanisms. A strategy to identify the unimportant reaction steps is to examine their normalized first-order sensitivity coefficients defined as

$$\frac{\left(\frac{\partial \ln X_k}{\partial \ln \alpha_i}\right)}{\max_i \left| \frac{\partial \ln X_k}{\partial \ln \alpha_i} \right|},\ or\ \frac{\left(\frac{\partial \ln T}{\partial \ln \alpha_i}\right)}{\max_i \left| \frac{\partial \ln T}{\partial \ln \alpha_i} \right|} \tag{4.2}$$

where X_k is the mole fraction of the k-th species, T is the temperature and α_i the pre-exponential factor (A) in the Arrhenius expression for the forward rate constant, $k_f = \alpha T^\beta \exp\left(\frac{-E_A}{RT}\right)$. A skeletal mechanism consists of only those reaction steps having sensitivity coefficients greater than a certain level, usually a 5% cut-off level.

The above criterion, when used alone, may have some shortcomings. The sensitivity coefficients are useful in identifying the "limiting" steps in chemical processes. If the chemical process occurs in a sequence, the slowest step can be identified by the

largest sensitivity coefficient. If the chemical process has several parallel steps, the largest sensitivity coefficient alone may not be sufficient in identifying the unimportant steps. The reason is that the fastest chemical step may have a fast reverse rate leading to a small net contribution to the production or destruction of the species. This situation is resolved by examining the normalized production or destruction rates. They are defined as,

normalized production value:

$$\overline{C}_{ki}^{p} = \frac{\max(\nu_{ki}, 0) q_i}{\sum_{i=1}^{I} \max(\nu_{ki}, 0) q_i} \tag{4.3}$$

normalized destruction value:

$$\overline{C}_{ki}^{d} = \frac{\min(\nu_{ki}, 0) q_i}{\sum_{i=1}^{I} \min(\nu_{ki}, 0) q_i} \tag{4.4}$$

where ν_{ki} is the stoichiometric coefficient of k-th species in i-th reaction, q_i is the rate of progress variable for the i-th reaction step, and I is the total number of reaction steps. It is possible that the first-order sensitivity coefficient of a species with respect to a certain reaction step is small although the corresponding normalized production or destruction value of that species is large. In other words, this particular reaction step would be eliminated by using only the sensitivity analysis. It is noted that reaction steps which are eliminated for the skeletal mechanism under the assumed flame condition (e.g.PSR) may become important under different conditions. Therefore, the applicability of the skeletal mechanism is limited to a specific range of conditions. The skeletal mechanism used in this work is called DRM22 (KAZAKOV and FRENKLACH (KAZAKOV and FRENKLACH)). It consists of 24 species and 104 elemental reactions.

4.3 Adaptive tabulation of combustion chemistry

As shown in section 3.5, for the reaction fractional step (equation (3.35)) the chemical source term $S(\phi)$ has to be integrated over the time step Δt. In combustion reactions, radical species such as OH or H are consumed very fast, there time scales are of the order of $10^{-10}s$ whereas pollutant species such as NO have time scales of the order of $1s$. For the chemical source term this means that the ratio between the

largest eigenvalue and the smallest eigenvalue is very large, for example 10^{10}. The ODE system

$$\frac{d\boldsymbol{\phi}}{dt} = S(\boldsymbol{\phi}) \tag{4.5}$$

is therefore called numerically stiff. The numerical integration of a stiff ODE system is numerically expensive. A typical steady-state PDF transport simulation may have 50000 cells, with 20 particles per cell and require 1000 iterations to converge. Hence, at least 10^9 stiff ODE integrations are required. Since each integration typically takes tens of milliseconds, the direct integration of the chemical source term is extremely CPU demanding.

A more efficient way would be to first solve the chemical source term for a set of representative initial conditions in composition space, and then to store the results in a pre-computed chemical lookup table. This operation can be described mathematically by a non-linear *reaction map*:

$$\boldsymbol{\phi}(\Delta t) = \boldsymbol{\phi}_{\Delta t} = \boldsymbol{R}(\boldsymbol{\phi}_0; t), \tag{4.6}$$

which is found by numerically integrating (4.5) over a time step Δt starting from initial composition $\boldsymbol{\phi}_0$. In order to construct the chemical lookup table, the reaction map $\boldsymbol{R}(\boldsymbol{\phi}_0; \Delta t)$ must be found for a set of representative points in composition space $\boldsymbol{\phi}_0^{[i]}$ $(i\ \varepsilon\ 1, ..., N_{tab})$. The chemical lookup table stores the updated values $\boldsymbol{\phi}_{\Delta t}^{[i]}$. Standard pre-computed lookup tables choose the representative points by computing the allowable region in composition space based on the inlet flow conditions and the kinetic scheme. The allowable region is determined by the constraints of the conservation of elements. The simplest method is to place these points on an (n_c)-dimensional grid in composition space. An important disadvantage of using a pre-computed lookup table is that it will contain many representative points that are never used in a particular transported PDF simulation. In contrast, *in situ* lookup tables store only the representative points which actually occur (accessed region) during the transported PDF simulation. FLUENT employs the ISAT method (POPE (1997)) to dynamically tabulate the chemistry mappings. ISAT (In-Situ Adaptive Tabulation) is a method to tabulate the accessed composition space region on-the-fly (in situ) with error control (adaptive tabulation).

At the start of a simulation, the ISAT table is empty. For the first particle reaction step, equation (3.35) is integrated with a stiff ODE solver. This is called a

direct integration (DI). The first table entry is created and consists of:

- the initial composition $\boldsymbol{\phi}_0$
- the mapping $\boldsymbol{\phi}_1 = \boldsymbol{\phi}_{\Delta t} = \boldsymbol{R}(\boldsymbol{\phi}_0; t)$
- the mapping gradient matrix $A = \dfrac{\partial \boldsymbol{\phi_1}}{\partial \boldsymbol{\phi_0}}$
- a hyper ellipsoid of accuracy

For the next particle reaction step, the initial composition vector is denoted $\boldsymbol{\phi}_0^q$, where the superscript q denotes a *query*. The existing table (consisting of one entry at this stage) is queried by interpolating the new mapping as

$$\boldsymbol{\phi}_1^q = \boldsymbol{\phi}_0^q + A\left(\boldsymbol{\phi}_0^q - \boldsymbol{\phi}_0\right). \tag{4.7}$$

The mapping gradient is hence used to linearly interpolate the table when queried. The region around the table point $\boldsymbol{\phi}_0$ in composition space where the linear approximation to the mapping is accurate is called the ellipsoid of accuracy (EOA). The size of the EOA is determined by one parameter, the tolerance ϵ_{tol}. If the query point $\boldsymbol{\phi}_0^q$ is within the EOA, then the linear interpolation by equation (4.7) is sufficiently accurate and the mapping is *retrieved*. Otherwise, a direct integration (DI) is performed and the mapping error $\epsilon = \left|B\left(\boldsymbol{\phi}_1^{DI} - \boldsymbol{\phi}_1^q\right)\right|$ is calculated. B is a scaling matrix, which takes into account that the rate of change in composition space might be different for different "directions". If the error is smaller than the specified error tolerance $\epsilon \leq \epsilon_{tol}$, then the original interpolation $\boldsymbol{\phi}_1^q$ is accurate and the EOA is *grown* so as to include $\boldsymbol{\phi}_0^q$. If not, a new table entry is *added* (see figure 4.1).

The table entries are stored as leaves in a binary tree. When a new table entry is added, the original leaf becomes a node with two leaves, the original leaf and the new entry. A cutting hyper-plane is created at the new node, so that the two leaves are on either side of the cutting plane. A composition vector $\boldsymbol{\phi}_0^q$ will hence lie on either side of this hyper-plane.

Since at the start of the simulation most operations are slow *adds* and *growths*, the first iterations are slow. Later in the simulation, as more of the composition space is tabulated, the faster *retrieves* become frequent and therefore the iteration time decreases. Simulation speed-ups of the order of 100 have been observed.

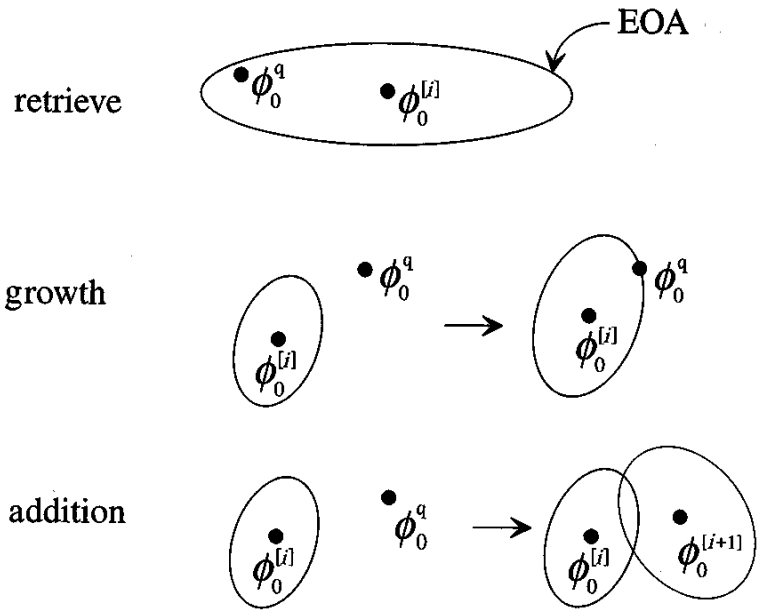

Figure 4.1: Sketch of the ellipsoid of accuracy

Chapter 5

The Delft III Flame

5.1 Introduction

Typical applications of non-premixed turbulent flames in combustion devices have large spatial scales. To be able to perform accurate measurements, smaller flames which can be investigated under laboratory conditions are needed. The *Delft piloted non-premixed flame burner* was designed to produce a number of well-defined, laboratory scale axisymmetric non-premixed turbulent flames. It was designed at the *Heat Transfer Section* of the *Technical University of Delft*. As the term "non-premixed" indicates, the fuel and oxidizer streams enter the combustion domain separately. This exhibits a main safety advantage over premixed systems, where a combustible mixture flow has to be formed before entering the combustion domain. The higher safety of non-premixed flames is one reason for the use of these flames in industrial scale applications.

The first part of this chapter describes the geometry of the Delft burner and the different fuel and air streams. Section 5.3 briefly describes the measurement techniques which have been used to obtain the experimental data. The chapter closes with a description of previously performed two dimensional simulations and the occurring problems.

5.2 Delft piloted non-premixed flame burner

5.2.1 Burner geometry

The burner consists of a central fuel pipe, surrounded by a primary air annulus. Figure 5.1 shows the burner head. The fuel jet nozzle is $6mm$ in diameter. It is separated from the primary air stream by a rim of outer diameter $15mm$. On this rim are twelve $0.5mm$ diameter holes located. The centers of the holes lie on a circle

with radius $3.5mm$. From these holes, a premixed acetylene/hydrogen/air mixture emerges which feeds the pilot flames. The outer diameter of the primary air annulus is $45mm$.

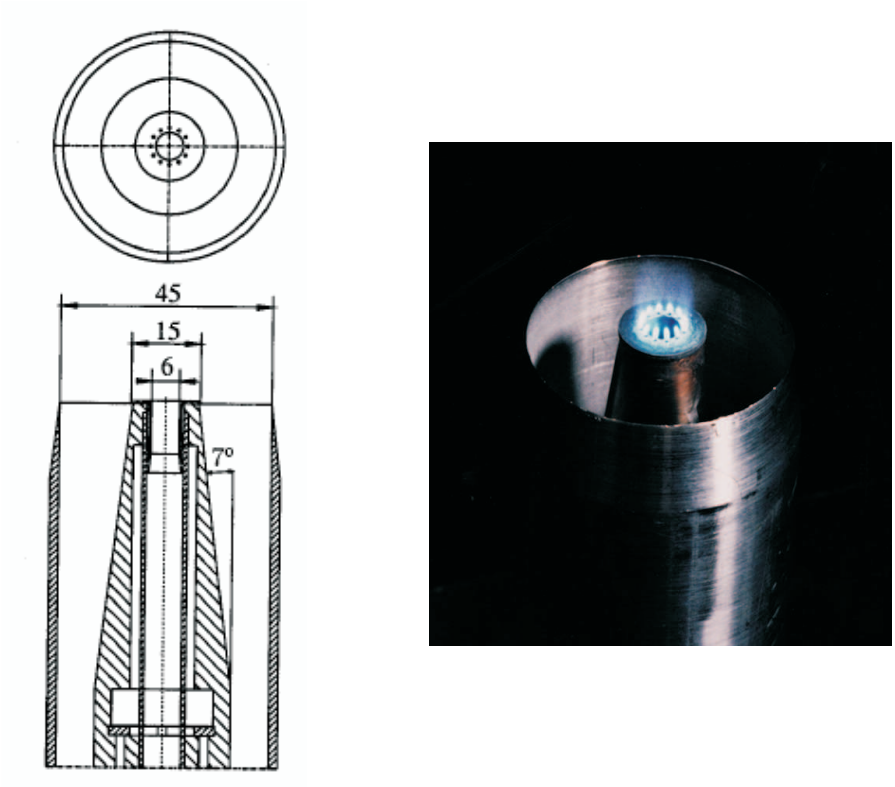

Figure 5.1: Left: Top and side view of the burner head. Dimensions in mm Right: photograph of burner head with pilot flames (Photograph courtesy of R.S. Barlow, Sandia National Laboratories).

The total length of the burner is $100cm$. In the first $94cm$, the inner diameter of the primary air annulus is $30mm$, decreasing to $15mm$ in the final $6cm$. This gives rise to a small negative radial velocity component of the primary air in the exit plane of the annulus. The initial diameter of the central fuel pipe is $8mm$. A pilot flame insert placed in the exit of the fuel pipe causes a decrease of the diameter to $6mm$ starting at a position $16mm$ upstream of the nozzle exit. Although the decrease in diameter is gradual with an $8°$ angle, the flow leaving the fuel pipe cannot be considered fully developed. To obtain reliable profiles at the burner exit plane, separate simulations of the fuel pipe and the air annulus have been performed. The

procedure is described in chapter 5. The burner is placed in a octagonal chamber, dimension $57cm$ from side to side. A low-velocity secondary air stream prevents a large-scale recirculation in the burner chamber.

5.2.2 Boundary conditions

At the University of Delft, experiments have been performed for six different flames. The different flames are all generated with the Delft burner using six different sets of inlet flow boundary conditions. The flow rates of fuel and air streams are varied to study the effect of different turbulent mixing rates. Table 5.1 gives an overview of the inlet boundary conditions of the six flames. For all flames, the secondary air stream is kept at room temperature, approximately $295K$, with a velocity of $0.4m/s$. The fuel used in the experiments is Dutch natural gas, consisting mainly of methane and nitrogen. The detailed composition and two simplified compositions are given in Table 4.1.

flame	Fuel jet			Primary air flow			L_f $[m]$
	U_{fuel} $[m/s]$	T_{fuel} $[K]$	Re_{fuel}	U_{ann} $[m/s]$	T_{ann} $[K]$	Re_{ann}	
I	11.0	295	4900	2.2	295	4400	0.87
II	15.4	295	6800	3.1	295	6200	0.9
III	21.9	295	9700	4.4	295	8800	0.85
IV	21.9	295	9700	8.0	295	16000	0.7
V	50.4	675	5300	11.2	654	5500	0.67
VI	49.6	664	5300	20.4	688	9300	0.52

Table 5.1: Inlet conditions for six different flames. U is the mean exit velocity, T the temperature and Re the Reynolds number. L_f is the visible flame length from DEVRIES (1994)

5.2.3 Pilot flames

The pilot flames are necessary to stabilize the non-premixed turbulent flame on the burner rim, especially in flames III and IV. The pilot flames are issued from twelve $0.5mm$ diameter holes, situated on a $7mm$ diameter ring on the rim separating the fuel and primary air streams, see figure 5.1. The pilot flames are

fed with an acetylene/hydrogene/air mixture. The composition of the mixture is:$Y_{H_2} = 0.01631,\ Y_{C_2H_2} = 0.07392,\ Y_{N_2} = 0.6983,\ Y_{O_2} = 0.211496$ and $T = 295K$. This mixture has the same C/H ratio as natural gas and an equivalence ratio of $\Phi = 1.4$. The exit velocity of the "pilot-jets" is $13.3m/s$ and the heat release in the pilot flames is about 1% of the total thermal power of Delft flame III.

5.3 Measurements of the Delft III flame

The flow field data for the different Delft flames have been measured at the Heat Transfer Section of the Delft University of Technology. The Laser Doppler Anemometry (LDA) was used and the data consists of mean and root mean square of the axial velocity and mean and root mean square of the radial velocity. The radial profiles of these quantities have been measured at various axial positions. The results of the LDA measurements are believed to be in Favre averaged form. Details of the measurements can be found in STROOMER (1995).

The latest measurements of scalar quantities have been performed in the Turbulent Diffusion Flame Laboratory of the Combustion Research Facility, Sandia National Laboratories, Livermore, USA. The Raman-Rayleigh-Laser-Induced-Florescence technique (Raman-Rayleigh-LIF) was used to measure the time and space resolved data on temperature and the concentrations of CO_2, O_2, CO, N_2, CH_4, H_2O, H_2, OH and NO. The relative random errors are estimated to lie between $1 - 12\%$. Details on the measurements can be found in NOOREN (1998) and the references therein. Figure 5.2 shows a photograph of the Delft III flame during the Raman-Rayleigh-LIF measurements.

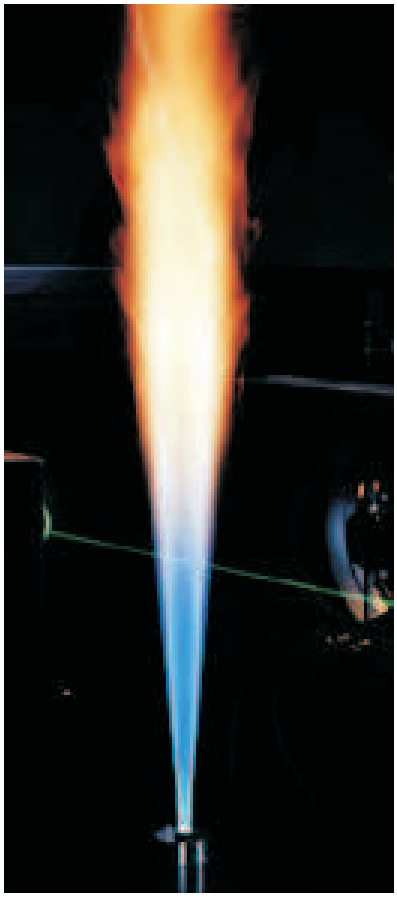

Figure 5.2: Photograph of flame III. The area covered is approximately 72 (height) × 25 (width) cm. (Courtesy of R.S. Barlow, Sandia National Laboratories).

5.4 Two-dimensional simulations of the Delft III flame

The Delft III flame has relatively strong interaction between turbulence and chemistry and it is therefore a challenge to model the turbulence-chemistry interaction. The Delft III flame is one of the target flames of the *International Workshop on Measurements and Computations of Turbulent Nonpremixed Flames (TNF)* (see www.ca.sandia.gov/TNF). The flame is very appropriate to study the influence

of different micro-mixing models as well as chemistry models. The two most detailed modelling studies published to date are the two-dimensional simulations of NOOREN et al. (1997) and MERCI et al. (2005). The simulations of MERCI et al. (2005) are also performed with FLUENT. The data-files of these simulations have been allocated by Prof. Bart Merci, Department of Flow, Heat and Combustion Mechanics, Ghent University, Ghent, Belgium. The data files have been used as a starting point in the development of a three-dimensional model.

The geometry of the Delft burner is axisymmetric, except for the holes for the pilot flames. This allows simplified simulations using two-dimensional axisymmetric solvers. Solving the governing equations in two dimensions reduces the simulation times extremely. The problem in all two-dimensional modelling approaches of the Delft III flame is the model of the pilot flames. The pilot flames are generated in twelve distinct holes situated on the burner rim. This geometry cannot be reproduced in two-dimensional simulations of the flame. In all two-dimensional simulations the pilot flames need somehow to be modelled. The purpose of pilot flames is simply to stabilize the main flame on the burner rim by constantly igniting combustible compositions in their surroundings. The total mass flow rate through the twelve holes is small ($\approx 2.98 \cdot 10^{-5} kg/s$) compared to the fuel ($\approx 4.9 \cdot 10^{-4} kg/s$) and air ($\approx 7.6 \cdot 10^{-3} kg/s$) inlets. Thus, the influence of the pilot flames on the global flow field of the flame is very small. Indeed, the spontaneous emissions of the pilot flames shows that the three-dimensional effects (the twelve distinct pilot flames) already disappear after a few millimeters (see figure 5.1). The product streams of the individual pilot flames then combine to form a cylindrically symmetric stream. As a consequence, the pilot flames are simply neglected in the conserved-scalar simulations of MERCI et al. (2005). This is possible, because in the conserved-scalar simulations a simple chemical equilibrium assumption is used to model the chemistry. The chemical time scales are assumed to be infinitely small, thus reaction takes place wherever the composition is near stoichiometric. The turbulent time scales have no direct influence on the chemical reactions and the flame is burning stably without the pilot flames. Due to the extremely simplified chemistry model, the results of these simulations are not accurate.

In the two-dimensional transported PDF (TPDF) simulation of MERCI et al. (2005) a C_1 skeletal chemical mechanism, including 16 species and 41 reactions, was

used. The chemistry model accounts for finite rate chemistry effects such as local extinction and therefore the flame does not ignite without including a model for the pilot flames. Including the pilot flame combustion was not possible, since the used C_1 skeletal mechanism does not describe the combustion reactions of the C_2 species acetylene, the fuel of the pilot flame mixture. The only way to somehow include the pilot flames would have been to inject the burnt product mixture of the pilot flames. The temperature and composition of the hot pilot products could be obtained from a simple chemical equilibrium analysis. The injection of the hot pilot product gases is the common procedure in most simulations of other piloted jet diffusion flames. For the Delft III flame this approach is not straightforward. The area of the twelve $0.5mm$ pilot holes would have to be smeared over an annular area with width $0.1mm$. This would have caused too small cells in the simulations of MERCI et al. (2005). If the width of the annular would have been taken to be the size of the smallest cell ($0.5mm$), then the correct mass and momentum flow rate could not have been correctly imposed at the same time. Another, general problem of the injection of the burnt pilot gases is the too high velocity resulting from the big density difference between cold and hot pilot mixture. To obtain the correct mass flow rate by injecting the burnt mixture, the velocity of the hot "pilot jets" would be $103m/s$. This value is too high compared to the values found in the three-dimensional simulation including the pilot combustion (see chapter 6). The reason is that the acceleration of the pilot jets due to the density difference is not only orientated in axial direction but also in radial direction. The injection of hot pilot products thus remains problematic in two-dimensional axisymmetric simulations as well as in three-dimensional simulations.

As it was described above, the influence of the pilot flames on the global flow field is very small and restricted to a region very close to the burner head. In the TPDF simulations of MERCI et al. (2005), the pilot flames are therefore modelled by adding a heat source in the region where the pilot flames are expected to burn. The experimental thermal power of the pilot flames ($\approx 200W$) is added in two different regions, to study the differences in the results.

$$\begin{aligned} &\textit{pilot model } Q_1 : 10mm < x < 20mm;\ 6mm < r < 8mm;\ Q = 2.3 \cdot 10^8 W/m^3 \\ &\textit{pilot model } Q_2 : 0mm < x < 20mm;\ 3.5mm < r < 7mm;\ Q = 8.7 \cdot 10^7 W/m^3 \end{aligned} \tag{5.1}$$

Adding the thermal power of the pilot flames was sufficient to obtain a stable

burning flame and the results in the far field are reasonable, but the differences in the results obtained with the two different pilot flame models are remarkable in the first $100mm$ of the simulated domain. The differences are a consequence of the unrealistic high temperatures in the regions where the heat source is applied. The high temperature is a result of the constant heat source. Modelling the pilot flames as a variable heat source would be a better way, but there is no experimental data available from the region of the pilot flames from which a non-uniformly distributed heat source could be constructed. Due to the lack of information about the pilot flames, the region where their thermal power should be applied can only be roughly estimated. To obtain a better insight into the processes that stabilizes the flame on the burner rim, three-dimensional simulations including the pilot flames are needed. From these simulations, a better model of the pilot flames for the two-dimensional simulations could be constructed.

Having results from a detailed three-dimensional simulation of the Delft III flame including the pilot flames would also allow a new modelling approach in two-dimensional simulation. From the results of the three-dimensional simulations, the axial position where the three-dimensional effects of the pilot flames vanishes could be determined. Then a new two-dimensional axisymmetric model could be constructed, starting at the axial position where the three-dimensional effects vanish. The profiles of the flow field variables as well as the scalar values at this axial position could be extracted from a cross-section of the three-dimensional model. These profiles could then be used as inlet boundary conditions in the two-dimensional model, thus overcoming the difficulties of modelling the pilot flames.

The detailed three-dimensional modelling approach of the Delft III flame is described in the next chapter.

Chapter 6

Three-dimensional simulation of the Delft III flame

6.1 Introduction

As described in section 5.4, the real geometry of the pilot flames can be included only in three dimensional simulations of the Delft III flame. The results of the three-dimensional simulations could be used to find a better model for the pilot flames in the two-dimensional axisymmetric simulations. This is one reason for the development of a three-dimensional model of the Delft III flame. Another reason is that the influence of three-dimensional effects, especially for the flame stabilization in the pilot flame region, is not known yet. The influence is assumed to be negligible, but certainty could be obtained from three-dimensional simulations or more detailed measurements of the pilot flame region.

The first section of this chapter presents a technique developed during this work, to evaluate the applicability of the DRM22 skeletal chemical mechanism in the simulations of the Delft III flame. The second section of this chapter presents the geometry of the three-dimensional model of the Delft III flame. Details on the computational grid are also presented. Section 6.4 shows whether the obtained inlet profiles for the velocity and turbulence of the fuel and primary air stream are realistic. In section 6.5 the applied boundary-conditions of the simulations are presented. Section 6.6 describes the difficulty of including the premixed pilot flames in a model for non-premixed combustion. The chapter closes with a description of the solution strategy.

6.2 Evaluation of the applicability of the DRM22 chemical mechanism

We had shown in section 4.1, that the use of a detailed chemical mechanism for the combustion of methane in a turbulent flow is numerically not tractable. The detailed mechanism has to be reduced to a smaller set of species and reactions, that still describe the chemical kinetics reasonably well. The detailed chemical mechanism is reduced under the assumption of a particular flame condition (see section 4.2), e.g. a perfectly stirred reactor using a particular equivalence ratio. The applicability of the reduced chemical mechanism under different flame conditions or with different equivalence ratios has to be tested by comparing the results with results obtained from the detailed mechanism. Yet, this comparison is just possible for simple flame simulations, where the detailed mechanism can be applied. These tests are done by the researcher who developed the reduced mechanism. Testing the applicability of a chemical mechanism for a particular turbulent combustion problem, where the detailed mechanism cannot be applied, has to be done by the modeler. Choosing an appropriate reduced mechanism is crucial for turbulent flame simulations. To avoid time consuming test simulations with different chemical mechanism, a simple method has be developed to investigate the applicability of chemical mechanisms for a particular turbulent combustion problem.

Most skeletal and reduced chemical mechanisms for combustion of methane are derived with the aim to be applied in turbulent combustion simulation and are therefore working well, especially if they include not only species with just one carbon atom (C_1-species) but also species with two carbon atoms (C_2-species). For the simulation of the Delft III flame it is essential to use a chemical mechanism that includes C_2 chemistry, since the fuel species in the pilot flames is acetylene (C_2H_2). The skeletal mechanism (DRM22) used in this work was developed with the aim to describe methane combustion (see KAZAKOV and FRENKLACH (KAZAKOV and FRENKLACH)). So, it has to be tested if the DRM22 mechanism is able to describe the combustion of acetylene under the flow conditions of the pilot flames. Since the transported PDF simulations are very time consuming, testing the mechanism within the PDF simulations is too time consuming. Also, if one wants to use a different mechanism, these slow simulations have to be repeated. To avoid this

procedure, an easier and faster test for the mechanism was developed.

The test programm for the chemical mechanism is based on a Damköhler number analysis. The Damköhler number can be defined (see FOX (2003)) as,

$$Da_\alpha = \frac{\tau_\phi}{\tau_\alpha} \tag{6.1}$$

where τ_ϕ is the turbulent mixing time scale and τ_α is the chemical time scale of species α. The turbulent mixing time scale can be defined as,

$$\tau_\phi = \frac{k}{C_\phi \epsilon} \tag{6.2}$$

where C_ϕ is the constant from the micro-mixing model. The value for τ_ϕ can be estimated from the flow conditions, or from a "cold flow" simulation of the flame under investigation without chemical reactions. In this work, the values for τ_ϕ in the pilot flames and in the main flame were obtained from a cold flow simulation. The chemical time scales can be defined in terms of the *eigenvalues* of the *Jacobian matrix* of the chemical source term. For example, for a system of n_s species, the $n_s \times n_s$ Jacobian matrix of the chemical source term is given by

$$\boldsymbol{J}(\boldsymbol{c}) = \frac{\partial \boldsymbol{S}_c}{\partial \boldsymbol{c}}(\boldsymbol{c}) \tag{6.3}$$

where $\boldsymbol{c}$ is the species concentration vector (unit e.g. $\left[\frac{mol}{m^3}\right]$) and $\boldsymbol{S}_c = \frac{d\boldsymbol{c}}{dt}$ is the chemical source term defined in concentration units. The species concentrations are related to the species mass fractions

$$c_k = \rho \frac{Y_k}{W_k}, \tag{6.4}$$

where W_k is the molecular weight of species k. The components of the Jacobian matrix will depend explicitly on the composition $\boldsymbol{c}$ and implicitly on the temperature and so will the eigenvalues. Denoting the eigenvalues of the Jacobian by $\mu_\alpha(\alpha \, \epsilon \, 1, ..., n_s)$, the chemical times scales can be defined as

$$\tau_\alpha = \frac{1}{\mid \mu_\alpha \mid}, \quad \alpha \, \epsilon \, 1, ..., n_s. \tag{6.5}$$

Thus, the chemical time scales will depend on the composition and temperature.

In the test program, the mixture composition $\boldsymbol{c}$ is an input data. For example, the premixed composition of the pilot flames is known a priori. The Jacobian matrix

is computed numerically for different temperatures using a simple forward difference scheme. Then the eigenvalues of the Jacobian matrices are calculated numerically. Since the Jacobian matrix is also numerically stiff, the HQR-algorithm is used to calculate the eigenvalues. The HQR-algorithm is especially appropriate for stiff matrices. Details about the HQR-algorithm can be found in PRESS et al. (1992). With the eigenvalues of the Jacobian, the chemical time scales for each species can be computed. As described above, the turbulent mixing time scale is found from a cold flow simulation of the Delft III flame. Using this turbulent mixing time scale and the definition of the chemical time scale, the Damköhler number for each species can be computed.

For non-reacting species like N_2, the corresponding eigenvalue in the Jacobian matrix of the chemical source term is zero. Therefore the Da number for such conserved species will be exactly zero too. For species which participate in very fast chemical reactions (small chem. time scales) the Da number will be high, e.g. $Da >> 1$. For species that react very slowly (large chem. time scale), the corresponding Da number will be very small, e.g. $Da << 1$. If the Da number of a species is of the order of one, e.g. $Da \approx 1$, then the reactions of this species have the same time scale as the mixing time scale and strong interaction between the chemical reactions and the turbulent flow field can be found. Using this knowledge, one can evaluate a chemical mechanism. The analysis of the Da numbers is applied below for the pilot flames and for a rich composition of the main flame.

Da-number analysis of the Pilot flames:

The cold, unburnt composition of the pilot flames is: $Y_{H_2} = 0.01631$, $Y_{C_2H_2} = 0.07392$, $Y_{N_2} = 0.6983$, $Y_{O_2} = 0.211496$. From a cold flow analysis, the turbulent mixing time scale can be found as $\tau_\phi = 0.0001$. The Da numbers for the species are calculated for different temperatures. Figure 6.1 shows the Da-numbers of hydrogen, oxygen and water. The very high values of the Da numbers of these species can be explained with the oxidation of hydrogen. The reaction $2H_2 + O_2 \longrightarrow 2H_2O$ is very fast at high temperatures and strongly exothermic. This reaction somehow keeps the temperature high enough until the slower oxidation of C_2H_2 is completed.

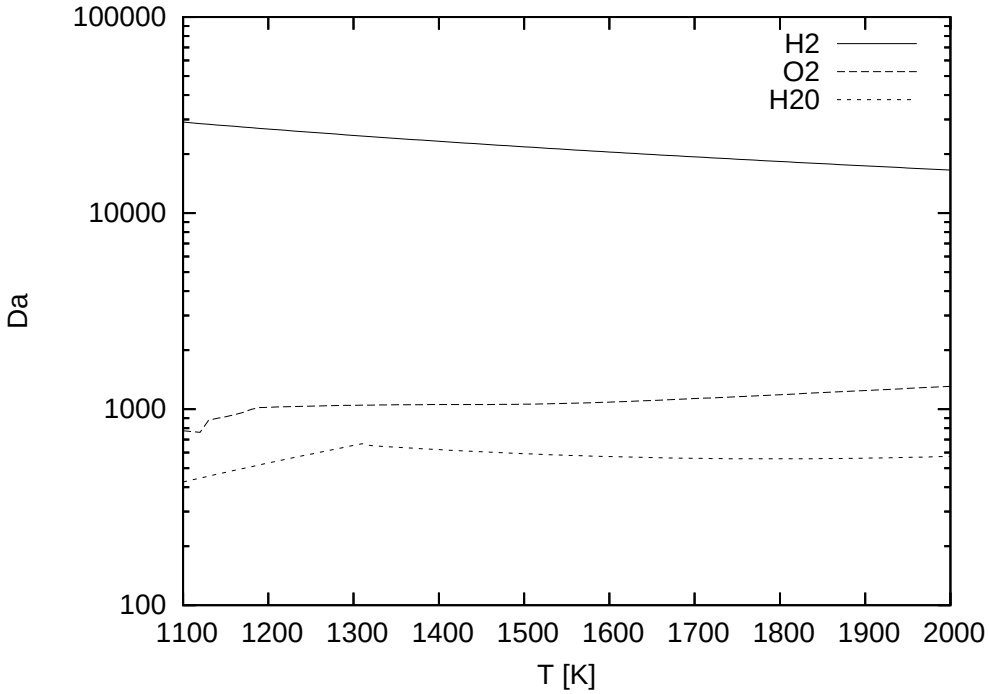

Figure 6.1: Da-numbers of hydrogen(H_2), oxygen(O_2) and water(H_2O)

In figure 6.2 the Da numbers of methane and some C_1 radicals are shown. It can be seen that the Da numbers of CH_2 and $CH_2(S)$ are high. Acetylene dissociates into gaseous and solid CH_2. $CH_2(S)$ is a main soot particle and it is well known that acetylene flames produce high amounts of soot under certain conditions. Due to recombination with H radicals, CH_4 and CH_3 are produced. The CH_3 and CH_2 radicals react mainly with O-radicals to CH_2O and CH_3O. These species are then converted to the stable end products CO and CO_2 (see figure 6.3).

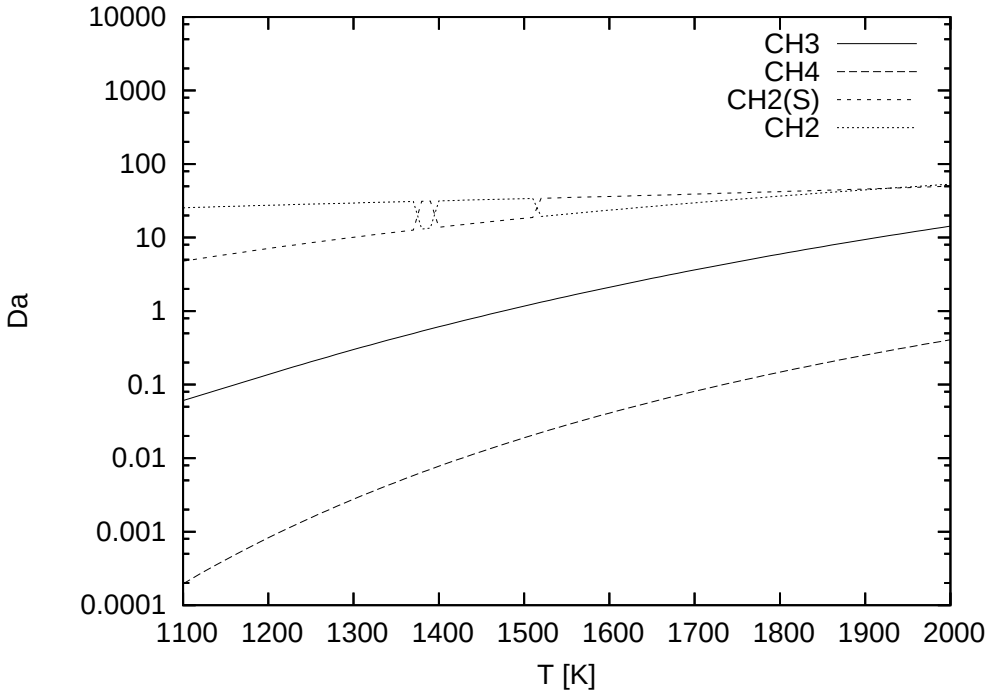

Figure 6.2: Da-numbers of methyl(CH_3), methane(CH_4), $CH_2(S)$, CH_2

As it can be seen from figure 6.3, the oxidation of methyl (CH_3) to CO and CO_2 is the slowest (low Da numbers) reaction step. This is in very good agreement with the theory of hydrocarbon combustion, see e.g. WARNATZ et al. (1996).

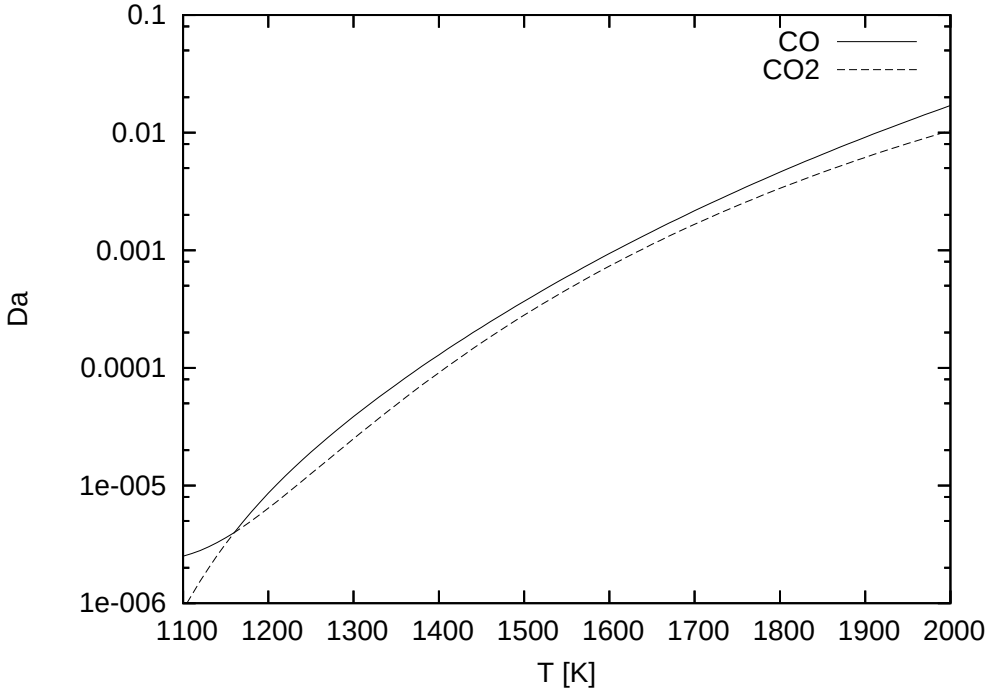

Figure 6.3: Da-numbers of carbon monoxide(CO) and carbon dioxide (CO_2)

Note that the Da number analysis does not show the progress of the reactions over time and it does not take the change of the composition into account. It shows somehow the relative importance of a species given a certain composition and mixing time scale. The figures 6.1-6.3 show that the DRM22 mechanism describes the main reaction steps in the oxidation of acetylene qualitatively correct. It also shows that the chemistry is fast enough to work under the flow conditions of the pilot flames.

Da-number analysis of the main flame, equivalence ratio $\Phi = 1.42$:

A conclusion from the two-dimensional simulations of the Delft III flame in MERCI et al. (2005) is that the quality of the transported PDF results depends on the ability of the chemical mechanism to describe the combustion of rich compositions accurately. To evaluate the DRM22 for rich combustion, the Damköhler number analysis is performed for a rich main fuel jet mixture. The composition and the mixing time scale are obtained from a cold flow simulation. The mixture composition is $Y_{CH_4} = 0.0652,\ Y_{C_2H_6} = 0.0059,\ Y_{N_2} = 0.7144,\ Y_{O_2} = 0.2,\ Y_{H_2O} = 0.0055,\ Y_{CO} = 0.003,\ Y_{CO_2} = 0.006$. Since this is the composition in a region close

to the pilot flames the same turbulent mixing time scale ($\tau_\phi = 0.0001$) as it was used for the pilot flame analysis is applied. Figure 6.4 shows the Da numbers of O_2, H_2 and H_2O. The Da numbers are again very high due to the hydrogen oxidation. This reaction is very fast and seems to be almost in chemical equilibrium.

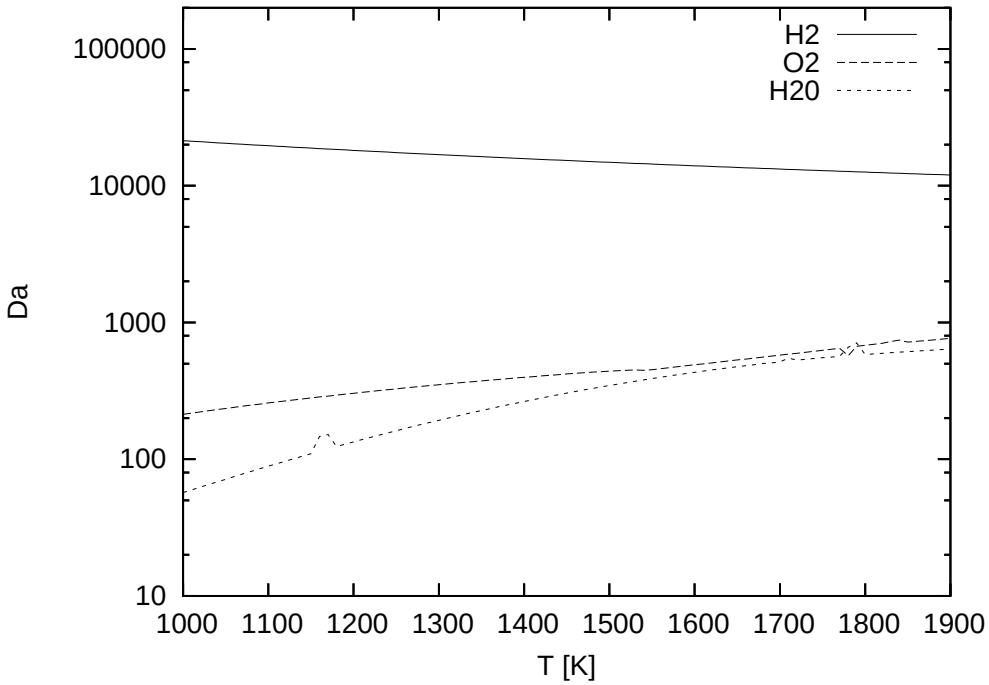

Figure 6.4: Da-numbers of hydrogen(H_2), oxygen(O_2) and water(H_2O)

In the figure 6.5 the Da numbers of the most important carbon species are shown. The methane molecules are converted to methyl radicals by loosing one hydrogen atom. For the combustion of methane, the CH_2 species is not as important as in the acetylene combustion and is therefore not shown. As it was found above, the oxidation of the methyl(CH_3) radical to CO and CO_2 is again the limiting reaction step. The Da numbers for the combustion of the methane air mixture are generally lower than the Da numbers of the acetylene combustion. This is mainly due to the lower temperature in the methane combustion.

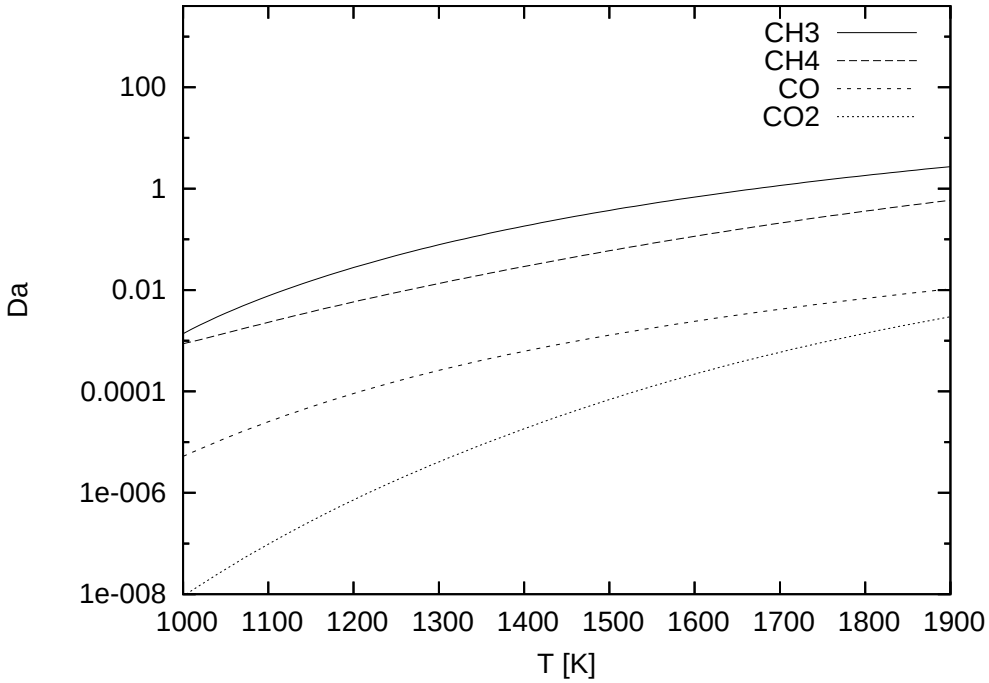

Figure 6.5: Da-numbers of CH_3, CH_4, CO_2 and CO

The results of the Da analysis for the rich methane-air combustion show again good agreement with the theory of hydrocarbon combustion.

The Da number analysis shows, that the DRM22 mechanism should be able to describe both, the acetylene combustion in the pilot flames and the methane air combustion in the main flame. Thus, the DRM22 mechanism is used for the transported PDF simulations.

6.3 Geometry of the three-dimensional model

The simulated domain extends up to $105mm$ in axial direction, to fully cover the region of influence of the pilot flames. The pilot flames need a very fine grid. Therefore, covering the whole domain in one simulation was computationally not tractable. To further reduce the simulation time, a sector of 90° was simulated instead of the whole circumference. This sector includes three pilot flames. The accuracy of the flow field obtained with this azimuthal extension was compared to the results obtained with a 180° sector. Almost no differences in the results have been found.

The computational domain of the model starts at the exit plane of the burner. In the model, the axial position of the burner exit plane is located at $x = -0.5mm$. This is because the burner rim (thickness $0.5mm$) is included in the model. The end of the rim is the exit plane of the fuel and pilot streams. Figure 6.6 shows a sketch of the computational domain.

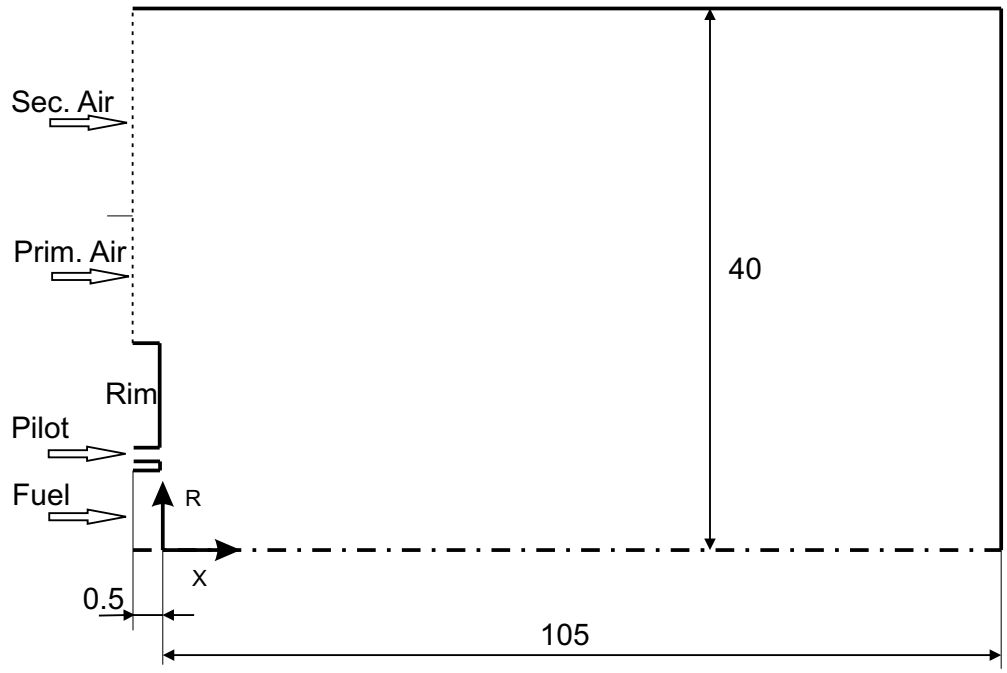

Figure 6.6: Sketch of the comp. domain and the inlet flows (dimensions in mm).

The size of the computational domain as well as the number of grid points are summarized in table 6.1. All cells are of the hexahedral type. The mesh was generated with GAMBIT, the meshing program of the FLUENT package.

property	axial	radial	azimuthal
extension	$-0.5mm \leq x \leq 105mm$	$0mm \leq r \leq 40mm$	90°
grid points	101	49	45
smallest cell length	$0.2mm$	$0.05mm$	$0.06mm$
largest cell length	$2.5mm$	$4mm$	$1mm$
total number of cells: **235153**			

Table 6.1: Grid and geometry data of three-dimensional model

6.4 Inlet flow profiles

To keep the computational domain as small as possible, the domain of the model starts at the exit plane of the burner head (see section 6.3). In order to obtain reliable velocity profiles of the fuel and primary air flow, separate calculations of these flows inside the burner have been performed. For the main fuel profile, simulations have been performed starting at an axial position $x = -176mm$ upstream of the burner exit plane. Figure 6.7 shows a sketch of the simulated fuel pipe.

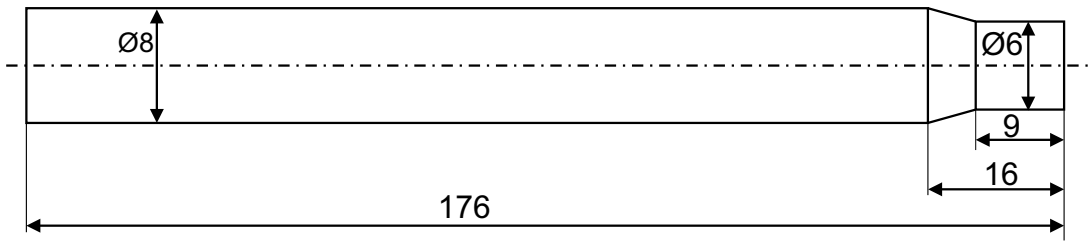

Figure 6.7: Sketch of the domain for the fuel pipe simulation (dimensions in mm)

The grid consists of 100 points in axial direction, 30 points in radial direction and 20 points in azimuthal direction. The y^+ values in all mentioned simulations are between 0.5 and 0.9. At the inlet, a uniform velocity of $12.2m/s$ is imposed and the density of the natural gas at $T = 295K$ is $\rho = 0.7664\frac{kg}{m^3}$. The length of the pipe before the constriction is long enough for the flow to reach a fully developed profile. However, due to the constriction, the flow at the exit is not fully developed and a

small radial velocity occurs. The mean axial and radial velocity, turbulent kinetic energy and turbulent dissipation rate, obtained at the fuel pipe exit are imposed as inlet boundary conditions for the flame simulations. The results are shown in figure 6.8.

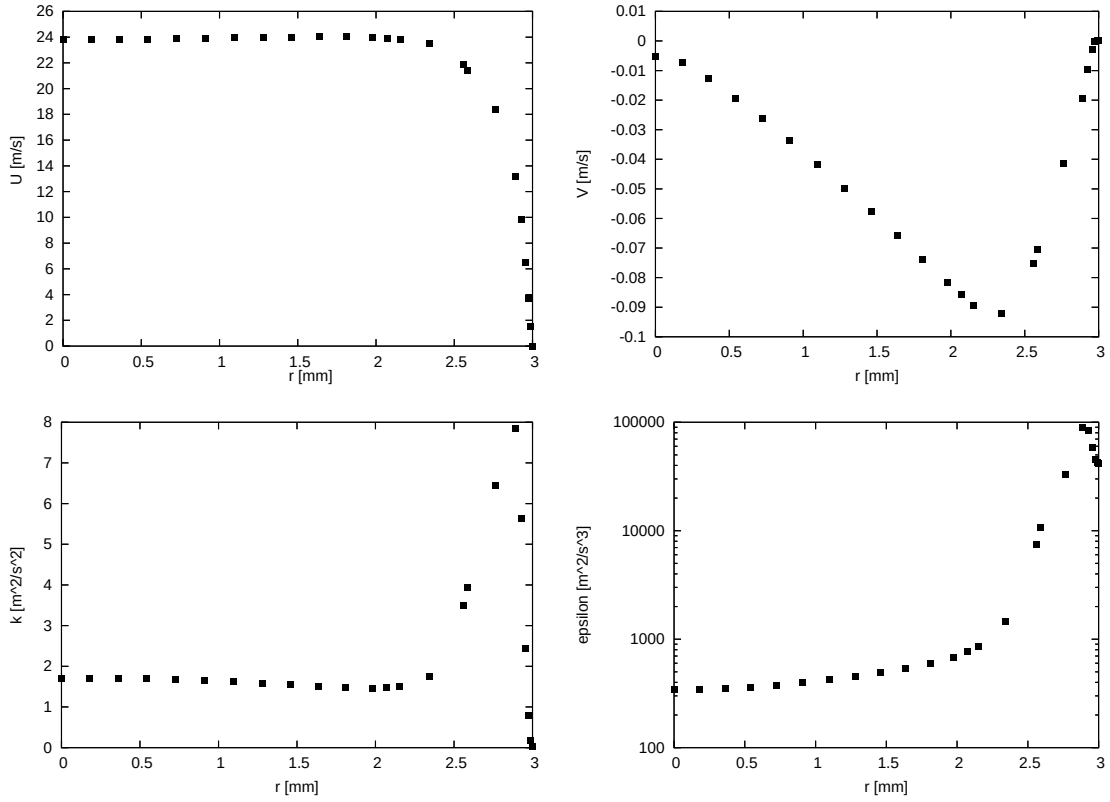

Figure 6.8: Radial profiles of mean axial and radial velocity (top), turbulent kinetic energy and turbulent dissipation rate (bottom) at the fuel pipe exit.

The profiles of the mean axial velocity, the turbulent kinetic energy and the turbulent dissipation rate show very good agreement with the theoretical prognosis. The non-zero mean radial velocity results from the constriction of the fuel pipe diameter from $8mm$ to $6mm$.

The flow through the whole primary air annulus was calculated in a separate simulation. The length is $100cm$ and the inner diameter decreases from $30mm$ to $15mm$ in the last $60mm$, see figure 5.1. The grid consists of 120 points in axial direction, 25 points in radial direction and 40 points in azimuthal direction. The velocity and turbulence profiles at the exit of the annulus are again imposed as inlet boundary conditions in the flame simulations. The results are shown in figure 6.9.

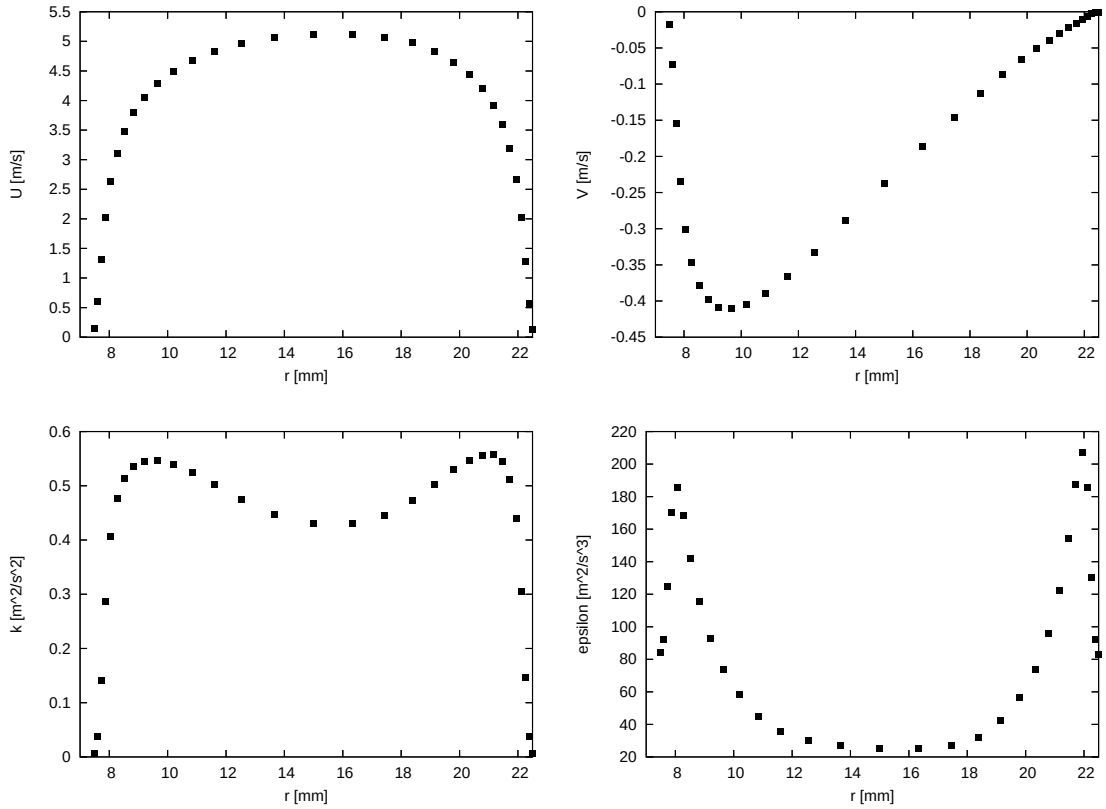

Figure 6.9: Radial profiles of mean axial and radial velocity (top), turbulent kinetic energy and turbulent dissipation rate (bottom) at the primary air annulus exit.

Again, the profiles of the mean axial velocity, the turbulent kinetic energy and the turbulent dissipation rate show very good agreement with the theoretical prognosis. The relatively high radial velocity is due to the decrease of the inner diameter from $30mm$ to $15mm$ in last $60mm$ of the air annulus (see figure 5.1).

For the secondary air stream, uniform profiles are imposed: $U = 0.4m/s$, $k = 6 \cdot 10^{-4}m^2/s^2$ and $\epsilon = 5.4 \cdot 10^{-5}m^2/s^3$.

6.5 Boundary conditions

In the three-dimensional simulations, velocity inlet, pressure outlet, periodic and solid wall boundary conditions (BC) have been used.

velocity inlet BC:

The flow inlets are defined through velocity inlet BC. The values for the mean axial, radial and tangential velocities as well as the scalar values are specified. The turbulence is specified either by directly defining the values of k and ϵ on the boundary or by defining the turbulence intensity and the hydraulic diameter. For the main fuel, the primary air and the secondary air inlet the profiles obtained from the simulations described above are imposed. For the three pilot inlets, an axial velocity of $13.3m/s$, a turbulence intensity of 0.5% and a hydraulic diameter of $0.5mm$ are used to specify the inlet.

wall BC:

The burner rim is modelled as a solid wall. The no-slip condition is applied as well as a zero heat flux condition. For the turbulence, standard near-wall functions are used. For a detailed description of the wall functions, see FLUENT (2005).

pressure outlet BC:

The flow outlets as well as the upper boundary in the three-dimensional simulations are modelled as pressure outlets. At a pressure outlet, the value of the static pressure is specified. To maintain numerical stability, FLUENT allows to specify values for the turbulence and scalars if "backflow" occurs at the boundary.

periodic BC:

Since the three-dimensional model consists only of a quarter of the real domain, periodic boundary conditions are applied at the sector faces. The pressure drop over the periodic planes is assumed to be zero. FLUENT treats the flow at a periodic boundary as if the opposing periodic plane were a direct neighbour to the cells adjacent to the first periodic boundary. Thus, when calculating the flow through the periodic boundary adjacent to a fluid cell, the flow conditions at the fluid cell adjacent to the opposite periodic plane are used.

6.6 Consideration of the premixed pilot flames

In this work, the combustion process of the pilot flames has been included for the first time in TPDF simulations of the Delft III flame. The difficulty in including the pilot flame combustion is that the pilot flames are of the premixed combustion type. This

means, fuel and oxidizer are homogeneously mixed prior to combustion. The physical and chemical processes of premixed combustion take place at different time and length scales as in non-premixed combustion. For example, in some circumstances a thin flame sheet (thinner than the Kolmogorov scale) forms a connected but highly wrinkled surface that separates the reactants from the products. Typically, the specific volume of the products is seven times that of the reactants, the flame surface being a volume source. All these effects, make a description of turbulent premixed combustion a difficult topic. Not many articles have been published over the last twenty years. In the work of POPE (1987) the difficulties of turbulent premixed combustion are summarized and the different types of premixed combustion are described. Using this characterization, the pilot flames are assumed to be of the distributed type (see POPE (1987) for details), because they are weakly turbulent and the finite rate chemistry introduces Da-numbers below unity. The Reynolds number of the pilot flames, built with the nozzle diameter $0.5mm$ as characteristic length scale, is $Re_D = 426$. This would suggest that the pilot jets are laminar, but the environment in which the pilot jets evolve is turbulent. The turbulent surrounding generates weak turbulence in the pilot jets.

In the recent work of MURA et al. (2002), a PDF modeling approach was presented, which is able to describe all types of turbulent premixed combustion. The problem is that turbulent non-premixed flames cannot be described with this approach. In order to include both, the premixed pilot flame and the non-premixed main flame combustion, in one simulation, one needs a model that can predict both types of combustion. For the simulations performed in this work, the TPDF model as described in section 3 was used. Using this model, the mixing constant C_ϕ of the mixing models (see section 3.4) had to be modified in order to obtain stable burning pilot flames. To obtain stable pilot flames, a high value for C_ϕ, e.g. $C_\phi = 20$ was used in the region of the pilot flames. The high C_ϕ value, decreases the mixing time scales in the pilot flame region to the values occurring in premixed combustion. This approach takes the correct physics into account, but the best approach would be a new mixing model, where the values of C_ϕ are calculated based on the flame conditions. The work on this new mixing model has already been started, but it is not completed yet and couldn't be used for the simulations presented in this work.

6.7 Solution approach

The transported PDF (TPDF) simulations are computationally very expensive. To start the simulations with this model would cause extremely long simulation times. An alternative way is to use simplified models first, to obtain a good initial solution of the flow field variables for the TPDF simulations. FLUENT allows to switch between different complex models for the combustion. This is one big advantage of using this CFD-package.

To obtain a stable solution, the idea was to imitate the ignition process of the real Delft III flame. To ignite the real flame, first the pilot and air flows are activated and the pilot flames are ignited using a match. Then the main fuel flow is activated and the main flame is ignited by the pilot flames. In the first simulation step, a result for the cold, non-reacting flow field and scalar values was obtained. Neglecting the chemistry greatly reduces the computational effort. For the next step, the calculation of the chemical reactions has been activated. The pilot flames have been "ignited" numerically by defining a high temperature value ($T > 1500K$) in the region where the fuel of the pilot flames (C_2H_2) was within certain limits ($0.02 \leq Y_{C_2H_2} \leq 0.07$). After stable burning pilot flames have been obtained, the main flame should have been ignited through the pilot flames, but this auto ignition of the main flame was not observed. To start the combustion process in the main flame, a high temperature value ($T > 1500K$) was defined where a combustible mixture of methane and oxygen was found.

Although stable burning pilot flames could be obtained and the combustion process in the main flame could be started, the pilot flames in the simulations could not stabilize the main flame on the burner head. After a few iterations, the main flame started to lift off from the burner head. The lifted main flame did not reach a steady-state and got extinguished finally. The results of the pilot flames and an explanation concerning instability of the main flame is given in the next chapter.

Chapter 7

Simulation results and final conclusions

7.1 Simulation settings

The best results of the pilot flames have been obtained with the Modified Curl mixing model and a locally varying value of C_ϕ. Details of the C_ϕ value can be found in table 7.1. The value $C_\phi = 4$ applied in the region of the main flame is somewhat higher than the standard value $C_\phi = 2$. The higher value was used, because in the simulations of NOOREN et al. (1997) an attached flame using the Modified Curl mixing model was obtained by increasing the value of the mixing constant to $C_\phi = 4$.

axial position	$0mm \leq x \leq 5mm$	$5mm < x \leq 10mm$	$10mm < x$
C_ϕ	20	$20 - (20 - 4)\frac{x - 5mm}{10mm - 5mm}$	4

Table 7.1: Values for C_ϕ

The model constants of the realizable $k - \epsilon$ model used in the simulations are shown in table 7.2. Standard values have been used except for the turbulent Schmidt number. The used value $Sc_t = 0.8$ is somewhat higher than the standard value $Sc_t = 0.7$. The reason for the higher value can be found in MERCI et al. (2005).

$C_{2\epsilon}$	*TKE Prandtl Number*	*TDR Prandtl Number*	*Turb. Schmidt Number*
1.9	1.0	1.2	0.8

Table 7.2: Model constants for the turbulence model

The absolute error for the direct integration in the ISAT table was set to 10^{-8}. The ISAT error tolerance was set to 0.0005, which is sufficiently small.

The general solution settings for the TPDF simulations in FLUENT are presented in table 7.3. The discretization method for the Finite Volume (FV) submodel is second order.

particles per cell	total number of particles	#PDF subiterations	#FV subiterations
20	$3.5 \cdot 10^6$	1	1

Table 7.3: Solution settings for the TPDF simulations

Increasing the amount of particles per cell had no significant influence on the results. A converged solution was obtained after 5000 iterations. The simulations have been performed on 10, 2.8GHz Opteron processors of the ISC (Institute for Scientific Computation) linux cluster at the University of Wyoming. The consumed CPU-time was approximately 50h.

7.2 Results

Figure 7.1 shows a contour plot of the mean static temperature in a cutting plane through a pilot flame.

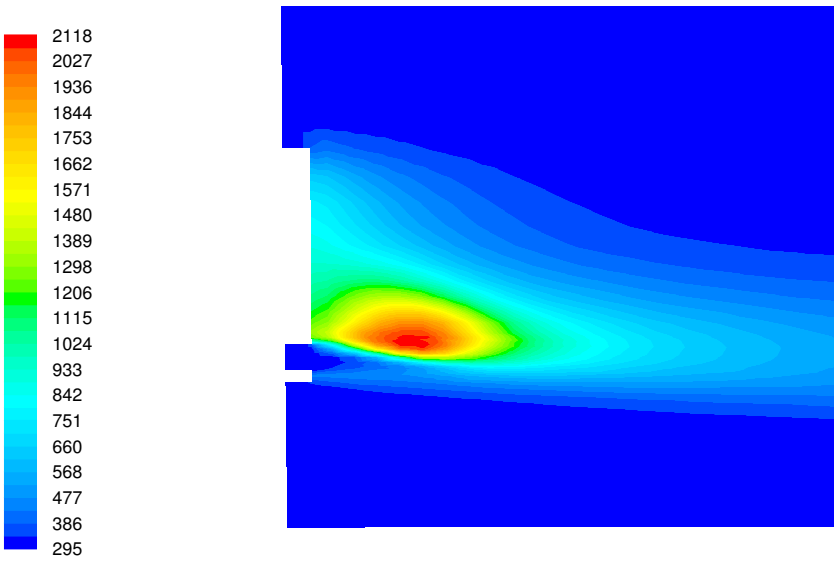

Figure 7.1: Contour plot of the mean static temperature [K].

Figure 7.1 shows, that the pilot flame is situated somewhat above the pilot exit plane. In this region, the velocity is smaller (see figure 7.2) and additional oxygen from the recirculation zone is available. The maximal temperature of $T_{max} = 2118K$ is lower than the temperature obtained from a chemical equilibrium analysis, $T_{equ} = 2375K$. This can be explained with the inclusion of finite rate chemistry effects in the TPDF simulations.

A contour plot of the mean axial velocity component in the same plane is shown in figure 7.2. It can be seen that the pilot jet gets "absorbed" by the main fuel jet at an axial position of $x \approx 3 - 4mm$. This is in good agreement with the spontaneous emissions of the pilot flames, shown in figure 5.1. The recirculation zone behind the burner rim is also visible in this contour plot.

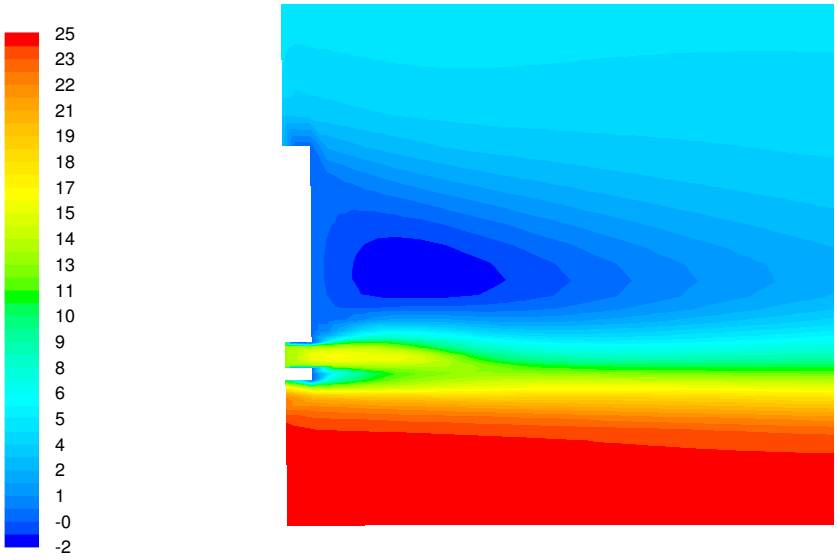

Figure 7.2: Contour plot of the mean axial velocity component [m/s].

In figure 7.3, contour plots of the mean static temperature and the mean axial velocity component in a radial plane at an axial position of $x = 4mm$ are shown. From these two contour plots, the axial position at which the distinct pilot flames combine together to form a cylindrically symmetric flow, can be estimated to $x \approx 4mm$.

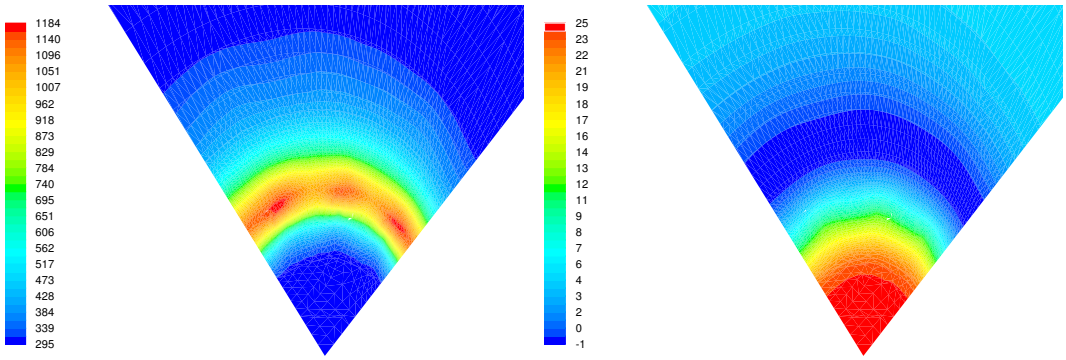

Figure 7.3: Contour plot of the mean static temperature [K] (left) and the mean axial velocity component [m/s] (right) in a radial plane located at $x = 4mm$.

The radial profiles of the mean axial velocity and the turbulent kinetic energy at an axial position $x = 3mm$ are presented in figure 7.4. The radial profiles are obtained in a plane which lies between two pilot flames. The simulation results are compared to the values obtained from the LDA-measurements.

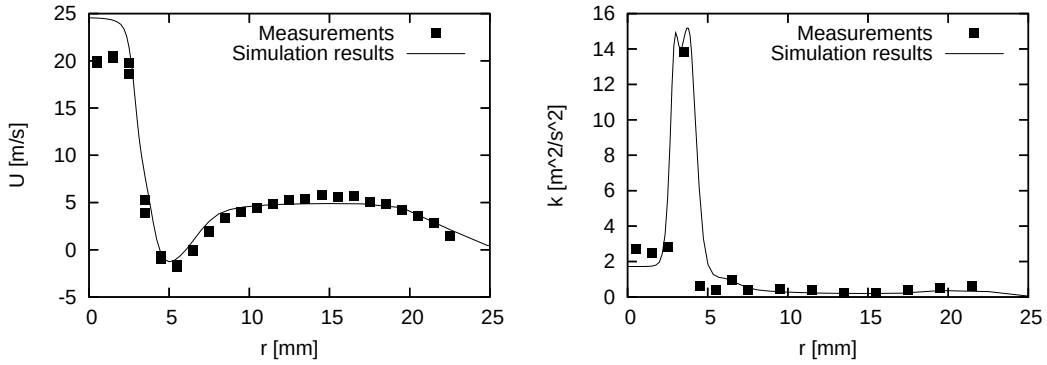

Figure 7.4: Radial profiles of mean axial velocity (left) and turbulent kinetic energy (right) at axial position x=3mm.

The results show good agreement with the experimental data. This is due to the fact, that the inlet profiles have been obtained from separated simulations on fine grids. The difference between simulation results and experimental data for the mean axial velocity at the center of the fuel is incomprehensively high. A reason for this difference could be, that the bulk velocity from which the fuel pipe mass flow rate was calculated, is slightly too high. The bulk velocity in the fuel pipe exit plane is $\overline{U} = 21.9m/s$, and can be found for example in MERCI et al. (2005). If the deceleration of the main fuel jet in the first $3mm$ is assumed to be negligible, then the mean axial velocity at $x = 3mm$ should be approximately the same as it was at the exit plane. The axial velocity profile in the fuel pipe exit plane is almost fully developed, as it was shown in section 6.4. In the mean axial velocity profile of a fully developed, turbulent pipe flow, the maximal velocity must be greater then the bulk velocity. A closer look at the experimental data shows, that the given bulk velocity value is greater than all measured values of mean axial velocity at $x = 3mm$. Therefore, the given bulk velocity might be too high.

In the experiments of the Delft III flame, an attached and stable burning flame has been observed. In the TPDF simulations, this state was observed only for a few iterations, after the main flame was ignited. After approx. 20 iterations, the

flame lifted off from the burner head and after approx. 300 iterations, the flame got finally extinguished. To obtain a stable burning flame, two conditions have to be satisfied. The pilot flames have to be simulated reasonably well and a combustible mixture of oxygen and methane is needed close to the pilot flames to be constantly ignited by the pilot flames. To show that a combustible mixture exists close to the pilot flames, the radial profile of the oxygen and methane mass fraction at an axial position $x = 5mm$ are presented in figure 7.5.

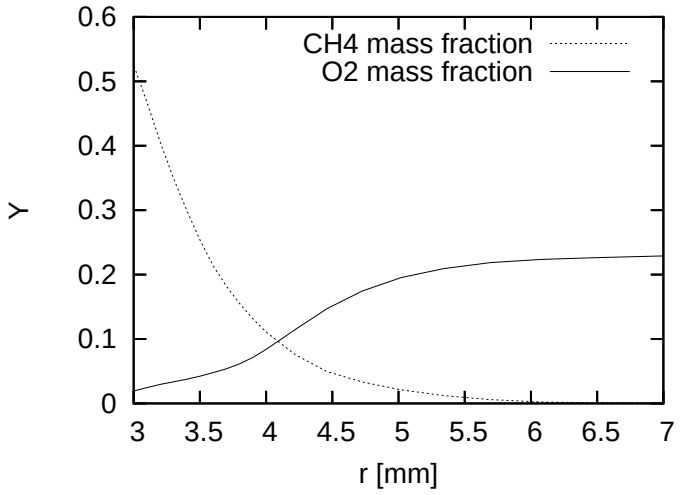

Figure 7.5: Radial profiles of the mean mass fraction for O_2 and CH_4 at an axial position $x = 4mm$.

In a combustible mixture, the oxygen and methane mass fractions have to lie between $Y_{CH_4} \geq 0.02, Y_{O_2} \geq 0.1$ and $Y_{CH_4} \leq 0.08, Y_{O_2} \leq 0.2$. The mixture between $r \approx 4.2mm$ and $r \approx 5.5mm$ is combustible.

In the region of the pilot flames, no experimental data of the scalar values is available. Thus, a quantitative evaluation of the simulation results for the pilot flames is not possible. To evaluate the efficiency of the combustion in the pilot flames, a contour plot of the acetylene mass fraction is shown in figure 7.6. Acetylene is the fuel of the pilot flames and the more unburnt acetylene is found, the less is the efficiency of the pilot flame combustion.

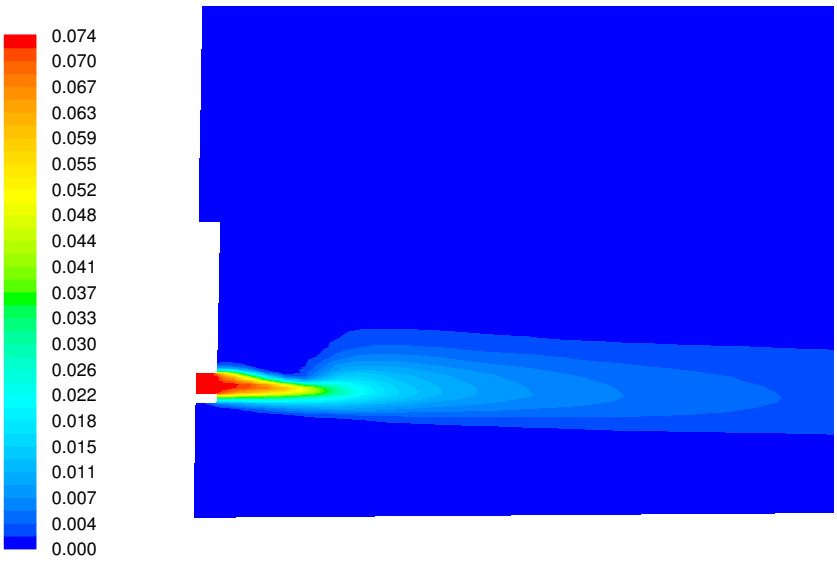

Figure 7.6: Contour plot of the mean mass fraction of acetylene.

As it can be seen in figure 7.6, only a small part of the acetylene is burnt at the upper side of the pilot jet. The thermal power released from the pilot flames is directly proportional to the mass flow rate of the burnt products. Only a small part, approximately 15% of the total pilot mass flow rate is burnt to hot products. Thus, only 15% of the thermal power of the pilot flames are released. This is assumed to be the main reason for not getting a stable burning main flame.

One reason for the insufficient combustion progress in the pilot flames can be found in the mixing model. The used Modified Curl model was developed to describe non-premixed combustion. To extend the model to premixed combustion, the mixing constant C_ϕ was set to a high value in the region of the premixed pilot flame combustion (see section 6.6). Although the extended model is able to describe the premixed combustion in the upper part of the pilot jets, it might not be accurate enough to describe the premixed combustion in the center of the pilot jets, where the velocity is much higher.

A second reason for the incomplete combustion in the pilot flames, could be wrong values for the turbulent kinetic energy and the turbulent dissipation rate in the pilot jets. The mixing time scale was defined as $\tau_\phi = \frac{k}{C_\phi \epsilon}$. Too high values for

ϵ together with the high value of the mixing constant $C_\phi = 20$ in this region could result in mixing time scales much smaller than the reaction time scales, no reaction would be possible. As described in section 6.6, the pilot jets are laminar. Since they evolve in a turbulent surrounding, small values for the turbulent kinetic energy and the turbulent dissipation rate are expected. In figure 7.7 contour plots of the turbulent kinetic energy and the turbulent dissipation rate are shown.

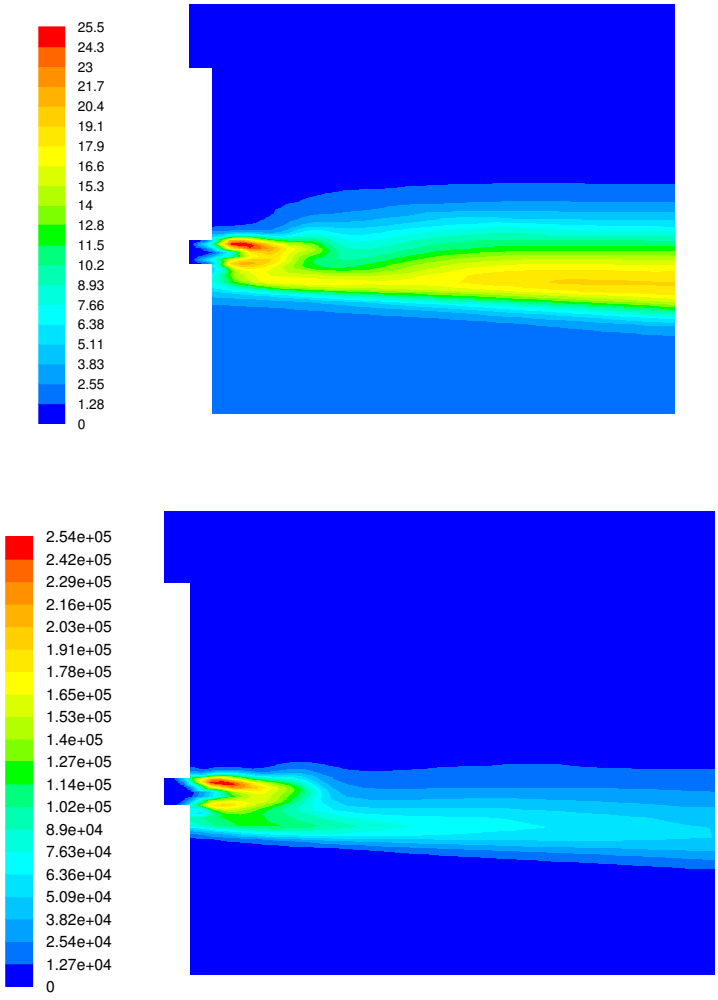

Figure 7.7: Contour plots of the turbulent kinetic energy $[m^2/s^2]$ (top) and turbulent dissipation rate $[m^2/s^3]$ (bottom) of a cold flow simulation

The contour plots are generated from simulation results for the cold flow without chemical reactions. No experimental data is available to verify these results, but the values for the turbulent kinetic energy and the turbulent dissipation rate are unreasonably high. An explanation for these high values can be found in the used $k-\epsilon$ turbulence model. The basic assumption in the $k-\epsilon$ model is the near-equilibrium assumption for the turbulent spectrum (see section 2.4). This assumption is justified in turbulent flows with high Reynolds numbers, but is generally wrong for low Reynolds number flows.

7.3 Final conclusions

The inclusion of the pilot flame combustion in the three-dimensional simulations of the Delft III flame is very difficult, but necessary to stabilize the main flame. The difficulties result mainly from the fact that the combustion in the pilot flames is of the premixed type and the combustion in the main flame is of the non-premixed type. Non-premixed combustion can be described with the transported PDF model (see chapter 3). The available mixing models to describe the molecular species mixing have been developed for non-premixed combustion. They cannot describe the premixed combustion in the pilot flames without modifications. To simulate the pilot flames and the main flame in one closed simulation, a new mixing model has to be developed which is able to describe premixed and non-premixed combustion. The two combustion processes are caused by different physical processes and have completely different time and length scales. Thus, developing the mixing model for combined premixed and non-premixed combustion is difficult and could not be finished during this work. When the new mixing model is available, it can easily be applied in the existing three-dimensional model and further simulations can be performed.

In order to include the premixed pilot flame combustion in the simulations performed during this work, an available mixing model was modified. The mixing constant was set to a high value ($C_\phi = 20$) in the region of the pilot flames. The high value of C_ϕ takes the much smaller mixing time scale in premixed combustion into account. Although stable burning pilot flames could be obtained in simulations with the Modified Curl model and variable C_ϕ, the main flame did not burn stably.

The reason for this result is that not enough pilot fuel was burnt and the heat release in the pilot flames was not sufficient to stabilize the main flame. In the simulations, the turbulent kinetic energy and the turbulent dissipation rate in the pilot jets were overpredicted. This is due to the fact that the Reynolds number in the pilot jet is low and the used $k-\epsilon$ turbulence model is unable to describe such low Reynolds number flows accurately. In the simulations, the too high values for the turbulent dissipation rate in the pilot jets together with the increased mixing constant could cause unrealistic small mixing time scales in the pilot jets. If the mixing time scales are much smaller than the chemical reaction time scales, reactions cannot occur. In further simulations, a way has to be found to overcome the wrong predictions for the turbulent kinetic energy and the turbulent dissipation rate. This could be done with a different turbulence model or parameter tuning in the used $k-\epsilon$ model.

As described above, the difficulty of including the pilot flame combustion in the three-dimensional model is the fact that the combustion processes in the main flame and the pilot flames are completely different, but have to be described with one model. One could overcome this problem by separating the pilot flame combustion and the main flame combustion into two simulations. In a first simulation, only the region close to the pilot flames is modelled. Since the pilot jets are laminar, no turbulence model would be needed and the laminar finite rate chemistry model could be applied. The results of the pilot flame simulation could then be used as inlet condition in a second simulation, where the main flame is modelled with the $k-\epsilon$ turbulence model and the composition PDF model. The problem of this modelling approach is that no smooth transition between the two simulations could be achieved. Also, although the pilot jets are laminar, they evolve in a turbulent surrounding. This fact would be neglected, if the first simulation of the pilot flames would be performed under laminar conditions.

The main conclusion of this work is that a new mixing model is needed to include the premixed pilot flame combustion in the simulation of the Delft III flame.

Bibliography

International Workshop on Measurements and Computations of Turbulent Non-premixed Flames (TNF). www.ca.sandia.gov.

CHEN, J. (1997). Development of reduced mechanisms for numerical modelling of turbulent combustion. *Workshop on "Numerical Aspects of Reduction in Chemical Kinetics" 115*, pp.487–514.

DEVRIES, J. (1994). *Study on turbulent fluctuations in diffusion flames using laser induced flouresence.* Ph. D. thesis, Technische Universitaet Delft, The Netherlands.

FERZIGER, J. and M. PERIC (2002). *Computational Methods for Fluid Dynamics* (3rd ed.). Berlin: Springer.

FLUENT (2005). *User Guide* (6.2 ed.). Lebanon, New Hampshire: Fluent Inc.

FOX, R. (2003). *Computational Models for Turbulent Reacting Flows* (1st ed.). Cambridge: Cambridge Univerity Press.

FRIEDRICH, R. (1999). *Modeling of Turbulence in Compressible Flows. In Transition, Turbulence and Combustion Modelling, edited by Hanifi, A., Alfredson, P.H., Johansson, A. V. and Hennisgson, D. S.* (first ed.). Dordrecht, Boston, London: Kluwer Academic Publishers (ERCOFTAC Series).

HEINZ, S. (2003a). On fokker-planck equations for turbulent reacting flows. part 1. probability density function for reynolds-averaged navierstokes equations. *Flow, Turbulence and Combustion 70*, 115–142.

HEINZ, S. (2003b). *Statistical Mechanics of Turbulent Flows* (first ed.). Berlin: Springer.

KAZAKOV, A. and M. FRENKLACH. *DRM22.* www.me.berkeley.edu/drm/.

KLOEDEN, P. and E. PLATEN (1999). *Numerical Solutions of stochastic Differential Equations* (3rd ed.). Berlin: Springer.

LAUNDER, B. and D. SPALDING (1972). *Mathematical models of Turbulence* (first ed.). London: Academic Press.

MERCI, B., B. NAUD, and D. ROEKAERTS (2005). Flow and mixing fields for transported scalar pdf of a piloted jet diffusion flame ('delft flame iii'). *Flow, Turbulence and Combustion (in press)*, –.

MURA, A., F. GALZIN, and R. BORGHI (2002). A unified pdf-flamlet model for turbulent premixed combustion. *Cobustion Science and Technology 175*, 1573–1609.

NOOREN, P. (1998). *Stochastic modeling of turbulent natural-gas flames*. Ph. D. thesis, Technische Universitaet Delft, The Netherlands.

NOOREN, P., H. WOUTERS, T. PEETERS, D. ROECKAERTS, U. MAAS, and D. Schmidt (1997). Monte carlo pdf modeling of a turbulent natural-gas diffusion flame. *Combust. Theory Modelling 1*, 79–96.

POPE, S. (1985). Pdf methods for turbulent reactive flows. *Progress in Energy and Combustion Science 11*, pp.119–192.

POPE, S. (1987). Turbulent premixed flames. *Annual Reviews Fluid Mechanics 19*, 237–270.

POPE, S. (1997). Computationally efficient implementation of combustion chemistry using a *in situ* adaptive tabulation. *Combustion Theory and Modelling 1*, pp.41–63.

POPE, S. (2003). *Turbulent Flows* (1st ed.). Cambridge: Cambridge Univerity Press.

POPE, S. and S. SUBRAMANIAM (1998). A mixing model for turbulent reactive flows based on euclidian minimum spanning trees. *Combustion and Flame 115*, pp.487–514.

PRESS, W., B. FLANNERY, and W. VETTERLING (1992). *NUMERICAL RECIPES IN C* (2nd ed.). Cambridge: Cambridge Univerity Press.

SHIH, T., W. LIOU, A. SHABBIR, Z. YANG, and J. ZHU (1995). A new $k - \epsilon$ eddy viscosity model for high reynolds number turbulent flows - model development and validation. *Computers Fluids 24*, 227–238.

SMITH, G., D. GOLDEN, and M. FRENKLACH. *Gri-Mech 3.0*. www.me.berkeley.edu/grimech.

STROOMER, P. (1995). *Turbulence and OH structures in flames*. Ph. D. thesis, Technische Universitaet Delft, The Netherlands.

WARNATZ, J., U. MAAS, and R. DIBBLE (1996). *Combustion* (second ed.). Berlin: Springer.

WOUTERS, H. (1998). *Lagrangian Models for Turbulent Reacting Flows*. Ph. D. thesis, Technische Universitaet Delft, The Netherlands.